Title

Noncanonical role of Golgi-associated macrophage TAZ in chronic inflammation and tumorigenesis.

Journal

Science Advances, 11(4)

Authors

Park, So

Ju, Sungeun

Lee, Jaehoon

et al.

Publication Date

2025-01-24

DOI

10.1126/sciadv.adq2395

Peer reviewed

CELL BIOLOGY

Noncanonical role of Golgi-associated macrophage TAZ in chronic inflammation and tumorigenesis

So Yeon Park[1], Sungeun Ju[2], Jaehoon Lee[1,3], Hwa-Ryeon Kim[1], Yujin Sub[4], Dong Jin Park[1], Seyeon Park[1], Doru Kwon[5], Hyeok Gu Kang[6], Ji Eun Shin[1], Dong Hyeon Kim[1], Ji Eun Paik[1], Seok Chan Cho[1], Hyeran Shim[1], Young-Joon Kim[1], Kun-Liang Guan[7], Kyung-Hee Chun[6], Junjeong Choi[5], Sang-Jun Ha[1], Heon Yung Gee[4], Jae-Seok Roe[1], Han-Woong Lee[1,3], Seung-Yeol Park[2], Hyun Woo Park[1]*

Until now, Hippo pathway–mediated nucleocytoplasmic translocation has been considered the primary mechanism by which yes-associated protein (YAP) and transcriptional co-activator with PDZ-binding motif (TAZ) transcriptional coactivators regulate cell proliferation and differentiation via transcriptional enhanced associate domain (TEAD)-mediated target gene expression. In this study, however, we found that TAZ, but not YAP, is associated with the Golgi apparatus in macrophages activated via Toll-like receptor ligands during the resolution phase of inflammation. Golgi-associated TAZ enhanced vesicle trafficking and secretion of proinflammatory cytokines in M1 macrophage independent of the Hippo pathway. Depletion of TAZ in tumor-associated macrophages promoted tumor growth by suppressing the recruitment of tumor-infiltrating lymphocytes. Moreover, in a diet-induced metabolic dysfunction–associated steatohepatitis model, macrophage-specific deletion of TAZ ameliorated liver inflammation and hepatic fibrosis. Thus, targeted therapies being developed against YAP/TAZ-TEAD are ineffective in macrophages. Together, our results introduce Golgi-associated TAZ as a potential molecular target for therapeutic intervention to treat tumor progression and chronic inflammatory diseases.

INTRODUCTION

YAP and its paralog TAZ are well-established transcriptional coactivators of the TEAD family transcription factors that serve as key nuclear effectors of the Hippo pathway in the context of cell proliferation, tissue regeneration, and metabolism (*1*–*4*). Although studied primarily in the context of solid tumor progression and stem cell differentiation (*5*), more recent studies have focused on the roles YAP/TAZ play in hematopoietic cells, such as macrophages or T cells, where they function in immunity and inflammatory disease (*6*–*14*). Currently, YAP/TAZ are thought to function in immune cells via similar mechanisms they use in nonhematopoietic cells: (i) Hippo pathway–mediated YAP/TAZ phosphorylation leading to nucleocytoplasmic shuttling and (ii) the subsequent activation of target gene transcription by the YAP/TAZ-TEAD complex (*15*, *16*). Here, we found a previously undescribed regulatory mechanism that involves Toll-like receptor (TLR)- and cytokine-mediated signaling pathways upstream of macrophage TAZ expression, and moreover, the atypical localization of TAZ at the Golgi compartment instead of the nucleus. These findings led us to investigate the distinct molecular mechanisms and physiological relevance of TAZ in macrophages.

Dysregulated inflammation contributes to the pathology of numerous diseases (*17*). Macrophages are key players in innate immunity that attack pathogens and modulate inflammatory responses (*18*). They participate in inflammatory pathways, such as inhibitor of nuclear factor κB kinase (IKK)/nuclear factor κB (NF-κB), c-Jun N-terminal kinase (JNK), and Janus kinase (JAK)/signal transducer and activator of transcription (STAT), by releasing inflammatory molecules like tumor necrosis factor–α (TNF-α), interleukin-6 (IL-6), and IL-1β (*19*, *20*) that contributes to the initiation of inflammation. Macrophages are not limited to the first-line defenses against pathogens and tissue damage; they also play critical roles in the resolution of inflammation and tissue repair (*21*, *22*). The dysregulation of these processes can prolong inflammation and contribute to chronic inflammatory diseases. Accordingly, macrophage-driven chronic inflammation is a key feature of pathologic conditions, such as cancer, type 2 diabetes, metabolic dysfunction–associated steatohepatitis (MASH), and fibrosis (*23*–*25*). When stimulated by various factors in their microenvironment, macrophages become polarized into two basic phenotypes, M1 and M2. M1 macrophages are proinflammatory and antitumorigenic, while M2 macrophages are anti-inflammatory and protumorigenic (*18*, *26*). In the present study, we establish TAZ as a Golgi-associated protein in M1 macrophages where it facilitates the trafficking and secretion of proinflammatory cytokines and promotes leukocyte infiltration, thereby prolonging inflammation.

Previous studies have yielded somewhat varied results regarding the role of the Hippo-YAP/TAZ pathway in the determination of the hematopoietic stem cell lineages, the differentiation of myeloid cells, and the polarization and function of macrophages (*5*, *8*–*14*). To date, therapeutic strategies based on canonical YAP/TAZ-TEAD regulation, such as the pharmacological blockade of YAP/TAZ-TEAD interactions or TEAD palmitoylation, have been proposed for treating cancer and inflammatory diseases (*27*–*29*). Predicting the outcome of TAZ inhibition and achieving proper control of these processes will require a careful cell type–specific clarification of the underlying mechanisms

[1]Department of Biochemistry, College of Life Science and Biotechnology, Brain Korea 21 Project, Yonsei University, Seoul 03722, Republic of Korea. [2]Department of Life Sciences, Pohang University of Science and Technology (POSTECH), Pohang 37673, Republic of Korea. [3]Gemcro Inc., Seoul 03722, Republic of Korea. [4]Department of Pharmacology, Graduate School of Medical Science, Brain Korea 21 Project, Yonsei University College of Medicine, Seoul 03722, Republic of Korea. [5]College of Pharmacy, Yonsei Institute of Pharmaceutical Sciences, Yonsei University, Incheon, Republic of Korea. [6]Department of Biochemistry and Molecular Biology, Yonsei University College of Medicine, Seoul, Republic of Korea. [7]School of Life Sciences, Westlake University, Hangzhou 310030, China.
*Corresponding author. Email: hwp003@yonsei.ac.kr

to target macrophage TAZ for the treatment of tumorigenesis and chronic inflammatory diseases.

RESULTS

TLR-mediated TAZ induction in macrophages during the resolution of inflammation

The transcriptional coactivators YAP and TAZ are downstream effectors of the Hippo pathway that control cell growth and differentiation by promoting the expression of TEAD transcription factor target genes (*1*–*4*). The hematopoietic lineages exhibit barely detectable amounts of YAP and TAZ at both the transcript and protein levels (*30*) (Fig. 1A). Comparing several nonmacrophage and macrophage cell lines, we found that, while TEAD or the Hippo kinase large tumor suppressor kinase (LATS) are evenly expressed across different cell types, YAP and TAZ were exclusively expressed in nonmacrophage cells (Fig. 1B).

To identify physiological conditions that evoke aberrant YAP or TAZ induction, we stimulated macrophages with various pattern recognition receptor ligands such as TLR and retinoic acid-inducible gene I (RIG-I)–like receptor agonists (*31*, *32*). We treated the macrophage cell line Raw264.7 with the TLR ligands lipopolysaccharides (LPS), poly(I:C), Pam3CSK4, 12-*O*-tetradecanoylphorbol 13-acetate (TPA), or *Escherichia coli* (Fig. 1, C to E). We validated the induction of TAZ through immunoblotting using various TAZ antibodies (fig. S1A). Although macrophage TLR activation induced substantial increases in TAZ mRNA and protein levels, we did not observe any increase in YAP levels under the same conditions (fig. S1B). In addition, TLR stimulation did not affect TAZ expression in nonmacrophage cell lines with high basal TAZ expression, such as breast cancer cells (fig. S1E). Next, we found that up-regulation of *TAZ* mRNA preceded TAZ protein accumulation without any accompanying chromatin modifications at *TAZ* promotor regions (fig. S1F). While genes like *Lcn2*, *Cxcl3*, and *Il1f9* were found to be up-regulated along with changes in chromatin structure (fig. S1, I and J), we identified genes such as *Mmp14* and *Il1b* that are enhanced without changes in chromatin structure similar to *Wwtr1* (*TAZ*) (fig. S1, G and H). These results indicate that macrophage TAZ accumulation is a consequence of *TAZ* gene transcription rather than enhanced protein stability.

We further confirmed this aberrant TAZ induction via immunofluorescent staining with multiple TAZ antibodies (Fig. 1F and fig. S1, C and D). Unexpectedly, rather than the conventional nuclear or cytoplasmic localization governed by Hippo pathway–mediated TAZ phosphorylation (*4*, *33*), we found that TLR stimulation induced a distinct localization of macrophage TAZ into a perinuclear pattern. In addition to Raw264.7 cells, we confirmed this TLR-mediated TAZ induction in bone marrow–derived macrophages (BMDMs) isolated from mice (Fig. 1G and fig. S1, K and L). In contrast to what we observed upon stimulation with TLR ligands, we did not observe TAZ accumulation upon simulation with RIG-1 agonists (*34*), such as poly(dA:dT), 5p-dsRNA, or 3p-hpRNA, which mediate antiviral host responses (Fig. 1H). Consistent with this, except for TLR activation by extracellular poly(I:C), the activation of macrophage RIG-I by transfected poly(I:C) did not induce TAZ expression (Fig. 1H). These results indicate that activation of TLRs, but not cytosolic nucleic acid sensors, promotes TAZ expression in macrophages.

Next, we asked whether TAZ in macrophages should be classified as an early-response gene, acutely controlled by the onset of inflammation, or a late-response gene, induced during the resolution phase of the inflammatory response. After TLR activation or TPA treatment, we observed a specific increase and maintenance of *TAZ* mRNA expression at late time points (e.g., 21 hours) (Fig. 1, I and J). Consistent with these results, we confirmed late TAZ protein accumulation that was sustained for 24 or 48 hours after macrophage activation (Fig. 1, K and L, and fig. S1M). Together, these results demonstrate that, although TAZ expression is barely detectable in macrophages under basal conditions, prolonged TLR activation induces TAZ expression during the resolution phase of inflammation.

Golgi localization and Hippo-independent regulation of TAZ in TLR-stimulated macrophages

Hippo pathway–dependent nucleocytoplasmic translocation is a well-established mechanism that controls TAZ function in the context of cell proliferation and differentiation (*1*–*4*, *33*). In nonmacrophage cells, such as mouse embryonic fibroblasts (MEFs), suppression of Hippo kinase triggers the activation and nuclear accumulation of TAZ via its dephosphorylation and nuclear accumulation, which then allows it to interact with TEAD transcription factors (Fig. 2A). In Raw264.7 macrophages, however, we observed via immunofluorescence staining that prolonged LPS or TPA treatment led to the perinuclear accumulation of TAZ protein, where it showed strong colocalization with the Golgi marker receptor binding cancer antigen expressed on SiSo cells (RCAS1) and Golgi matrix protein 130 kDa (GM130) (Fig. 2B and fig. S2A). Furthermore, we confirmed that TAZ is localized to the cis-Golgi in Raw264.7 cells, as indicated by its colocalization with cis-Golgi marker GM130, but to less extent with trans-Golgi marker TGN38 (Fig. 2C and fig. S2, B to D). Consistent with these results, BMDMs and hMDMs stimulated with LPS or TPA showed marked accumulation of TAZ in GM130- and RCAS1-positive Golgi compartments (Fig. 2D and fig. S2, E and F). Further, we confirmed the exclusive localization of TAZ to the cytoplasmic region via fractionation assay performed with both Raw264.7 cells and BMDMs (Fig. 2, E and F). We clearly demonstrated the precise subcellular localization of TAZ at the Golgi by performing sucrose density gradient centrifugation and isolating a pure fraction containing the Golgi compartment (Fig. 2, G and H). These results establish macrophage TAZ as a Golgi-associated protein.

Next, we asked whether the Hippo pathway acts upstream of TAZ in macrophages. In nonmacrophage cells, such as MEF cells, the addition or withdrawal of serum elicits LATS1/2-mediated TAZ phosphorylation and nucleocytoplasmic translocation (Fig. 2I). In macrophages, however, neither serum starvation nor stimulation substantially altered the accumulation or localization of TAZ at the Golgi (Fig. 2J). In addition, although treatment with statins or LatB typically inhibits TAZ in nonmacrophage cells (*35*, *36*), we did not observe any LATS1/2-mediated phosphorylation of TAZ in macrophages (Fig. 2K). These results indicate that the Golgi-associated TAZ in macrophages does not respond to typical Hippo pathway–related stimuli.

Next, to determine whether TAZ acts as a transcriptional coactivator of TEAD, we investigated protein-protein interactions between TAZ and TEAD in activated macrophages. In contrast to MEF cells, which showed a strong interaction between TAZ and TEAD, Golgi-associated TAZ did not bind to TEAD in macrophages (Fig. 2L). Unexpectedly, by performing fractionation assay and immunofluorescent staining experiments, we found in both Raw264.7 and BMDM cells that TEAD itself was localized and diffused in the

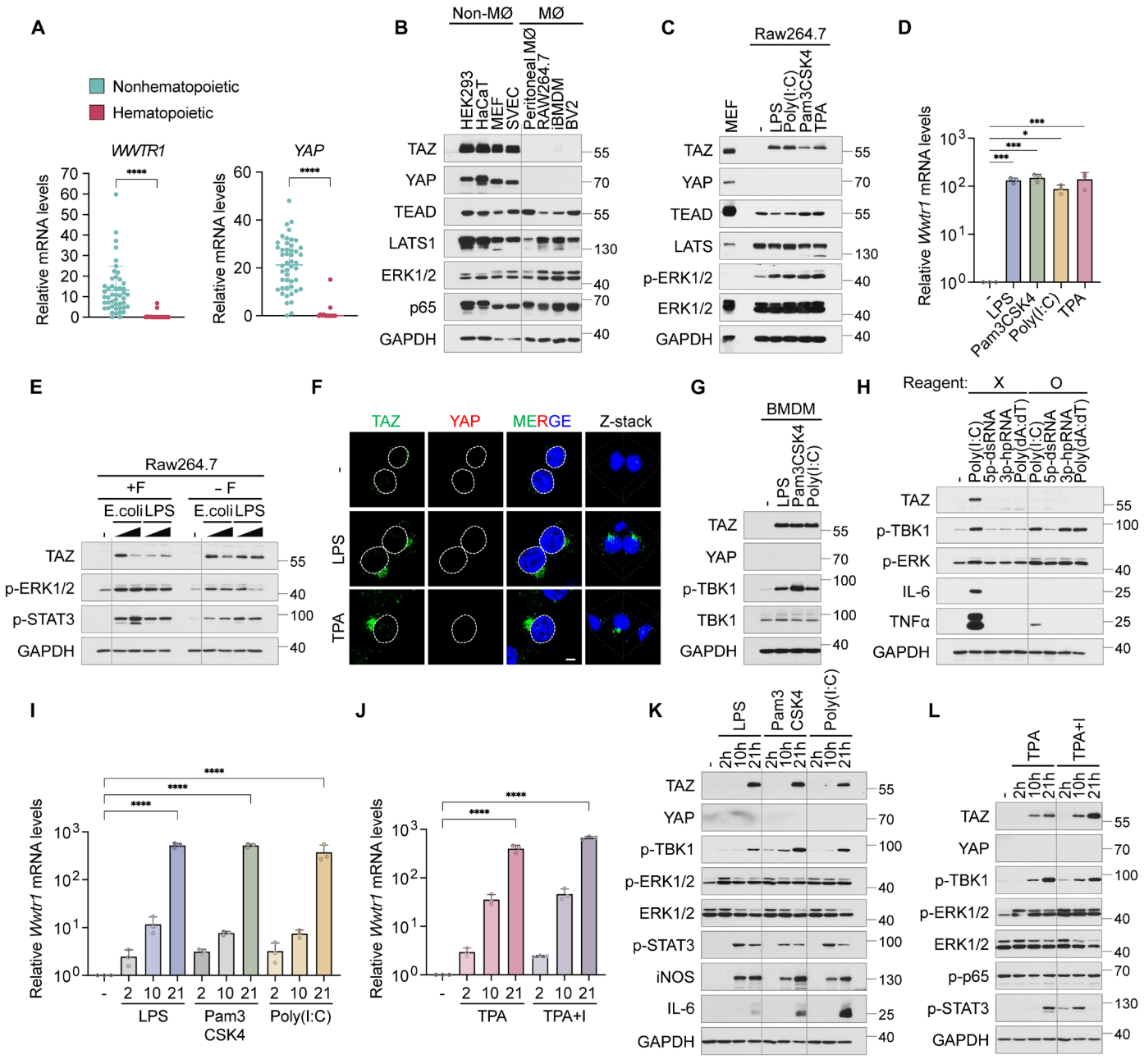

Fig. 1. TLR-mediated TAZ induction in macrophages during the resolution of inflammation. (**A**) *WWTR1* (*TAZ*) and *YAP* mRNA levels in adherent ($n = 47$) and hematopoietic ($n = 17$) cell lines were analyzed using Human Protein Atlas data and processed using Student's *t* tests. ****$P < 0.0001$. GAPDH, glyceraldehyde-3-phosphate dehydrogenase. (**B**) Immunoblotting compared protein expression between nonmacrophage [human embryonic kidney (HEK) 293, HaCaT, mouse embryonic fibroblast (MEF), and SVEC] and macrophage (peritoneal macrophages, Raw264.7, iBMDM, and BV2) cell lines. (**C**) Immunoblotting analyzed TAZ expression in Raw264.7 cells with LPS (100 ng/ml), Pam3CSK4 (100 ng/ml), Poly(I:C) (50 ng/ml), or TPA (100 nM) for 16 hours, with MEF as a control. (**D**) qPCR analysis of *TAZ* mRNA in Raw264.7 cells treated with LPS (100 ng/ml), Pam3CSK4 (100 ng/ml), Poly(I:C) (50 ng/ml), or TPA (100 nM) for 16 hours. One-way analysis of variance (ANOVA) with Bonferroni tests. *$P < 0.05$, ***$P < 0.001$. (**E**) Immunoblotting analysis of TAZ expression in Raw264.7 cells treated with *E. coli* (2×10^6 CFU/ml and 6×10^6 CFU/ml) or LPS (100 or 300 ng/ml) for 16 hours. (**F**) Immunofluorescence images of TAZ (green) and YAP (red) in Raw264.7 cells treated with LPS (100 ng/ml) or TPA (100 nM) for 16 hours. Three dimensional confocal reconstructions included. Scale bar, 3 μm. (**G**) Immunoblotting analysis of TAZ expression in BMDMs treated with LPS (100 ng/ml), Pam3CSK4 (100 ng/ml), or Poly(I:C) (50 ng/ml) with or without serum for 24 hours. (**H**) Immunoblotting analysis of TAZ expression in Raw264.7 cells treated with Poly(I:C) or the RIG-I agonists poly(dA:dT), 5p-dsRNA, or 3p-hpRNA with or without transfection reagent for 24 hours. (**I** to **L**) TAZ mRNA and protein levels were measured in Raw264.7 cells treated with LPS (100 ng/ml), Poly(I:C) (50 ng/ml), Pam3CSK4 (100 ng/ml), TPA(100 nM) or TPA + ionomycin (1 μg/ml) for 2, 10, or 21 hours. The data were analyzed by one-way ANOVA with Bonferroni tests for multiple comparisons. ****$P < 0.0001$.

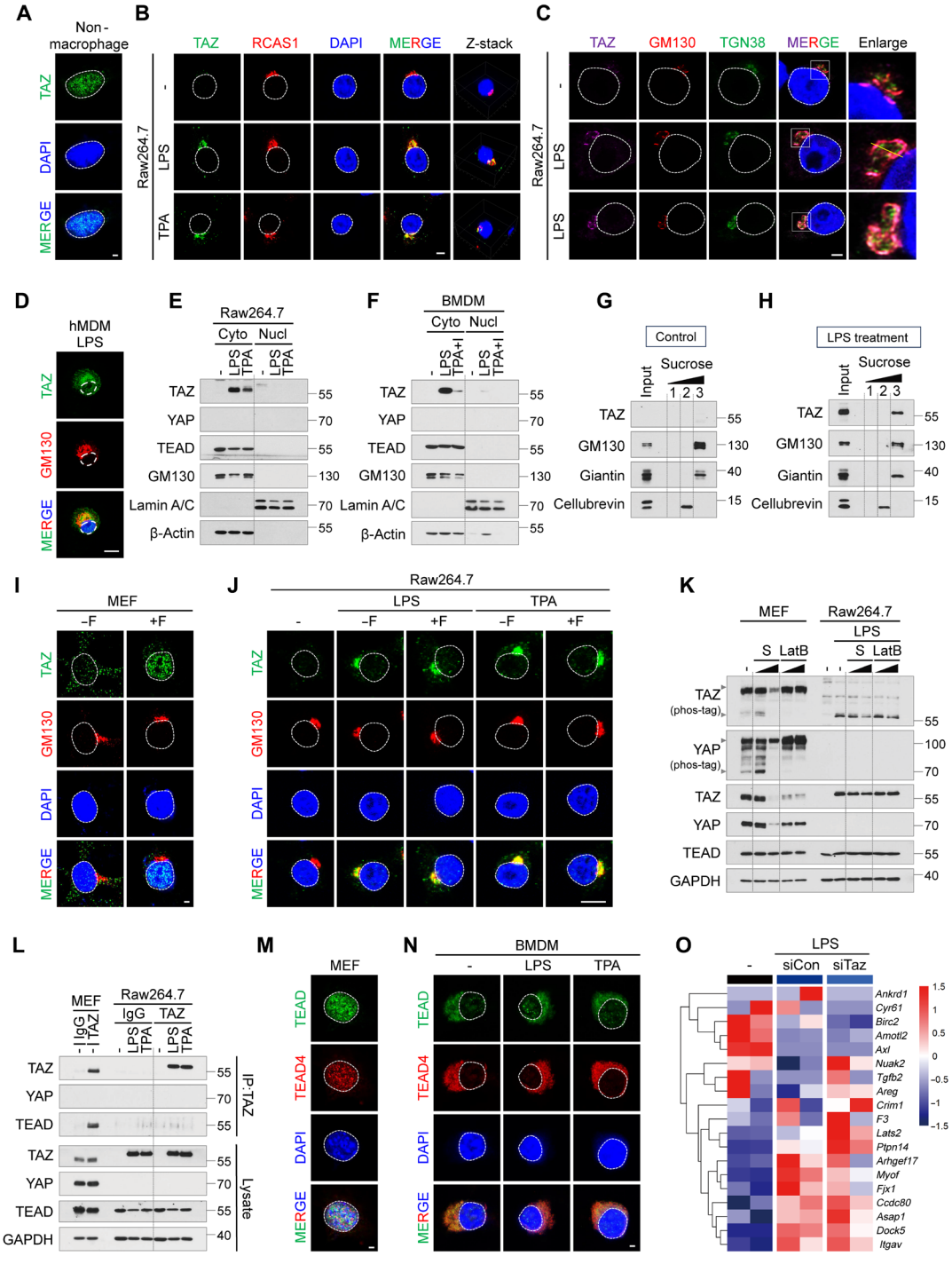

Fig. 2. Golgi localization and Hippo-independent regulation of TAZ in activated macrophages. (**A** to **D**) Immunofluorescence images show TAZ localization: (A) TAZ (green) in the nucleus of MEF cells; (B) TAZ (green) and RCAS1 (red) in Raw264.7 cells treated with LPS or TPA for 16 hours; (C) TAZ (magenta), GM130 (red), and TGN38 (green) in Raw264.7 cells treated with LPS for 16 hours; (D) TAZ (green) and GM130 (red) in hMDMs treated with LPS for 24 hours. Scale bars, 3 μm (A to C) and 10 μm (D). (**E** and **F**) Immunoblotting analysis of cytoplasmic and nuclear fractions in Raw264.7 (E) and BMDM (F) cells treated with LPS or TPA for 16 hours. β-Actin/Lamin A/C: cytosolic/nuclear markers. (**G** and **H**) Immunoblotting of Golgi fractions in Raw264.7 cells treated with or without LPS for 16 hours. (**I**) Immunofluorescence images showing TAZ (green) and GM130 (red) in MEF cells with or without serum. Scale bar, 3 μm. (**J**) TAZ (green) and GM130 (red) localization in Raw264.7 cells treated with LPS or TPA with or without serum. Scale bar, 15 μm. (**K**) Immunoblotting of TAZ phosphorylation status in MEF or Raw264.7 cells pretreated with TAZ inhibitors, statin (0.5 and 1 μM), or Lat B (0.1 and 0.2 μg/ml). Upper and lower arrowheads show phosphorylated and dephosphorylated TAZ and YAP. (**L**) Immunoblotting and Co-IP analysis of TAZ in MEF and Raw264.7 cells treated with LPS or TPA. (**M** and **N**) Immunofluorescence of pan-TEAD (green) and TEAD4 (red) in MEF cells (M) and BMDMs treated with LPS or TPA (N). Scale bar, 3 μm. (**O**) Heatmap from RNA sequencing (RNA-seq) data shows canonical TAZ/YAP-TEAD target gene expression in Raw264.7 cells treated with or without LPS in siControl- or siTaz-transfected cells. [(A) to (O)] All experiments used LPS (100 ng/ml) and TPA (100 nM).

cytoplasm rather than the nucleus (Fig. 2, E, F, and N). Thus, macrophage nuclei seem to lack all Hippo pathway effectors, including YAP/TAZ and TEAD. These results are distinct from previous reports obtained from nonmacrophage cells consistently demonstrating a nuclear localization of the TAZ-TEAD complex (Fig. 2M). They are also inconsistent with several studies suggesting a transcriptional role for YAP/TAZ and TEAD in activated macrophages (*10*–*12*). We further tested whether macrophage TAZ participates in the transcriptional activity of TEAD after LPS treatment. Although LPS treatment altered the expression of several known TEAD target genes, TAZ depletion did not affect their expression level, suggesting a transcription-independent function for macrophage TAZ (Fig. 2O). Small-molecule TEAD inhibitors that target either the YAP-TAZ-TEAD interaction or TEAD palmitoylation are being intensively developed as therapeutics in the context of tumorigenesis, inflammation, and regenerative medicine (*27*–*29*). Consistent with these results, while the TEAD inhibitors VT-104 and IK-930, which are in clinical trials, suppressed the canonical TEAD target genes *Ctgf* and *Cyr61* in Hippo-mutant cancer cells (*37*, *38*) (Fig. 3, A and B), they did not suppress the same genes in macrophages, nor did they suppress LPS-induced cytokine expression (Fig. 3, C to E). In addition to previous studies related to transcription-independent role of YAP/TAZ (*39*), to our knowledge, our results provide evidence of transcription-independent function of TAZ as a Golgi-associated protein in activated macrophages.

Golgi-associated TAZ-mediated regulation of proinflammatory cytokine secretion in M1

A variety of factors can polarize macrophages into either the M1 or M2 types, each of which participate in distinct inflammatory responses (*18*, *26*). To verify the function of TAZ, we tested whether TAZ expression was associated with a specific type of polarized macrophage. Proinflammatory M1 macrophages are induced by treatment with LPS and interferon-γ (IFN-γ) and recognized by their expression of inducible nitric oxide synthase (iNOS). Anti-inflammatory M2 macrophages are induced by treatment with IL-4 and IL-13 and recognized by their expression of arginase-1 and p-STAT6 (Fig. 4, A and B). Both Raw264.7 cells and BMDMs showed

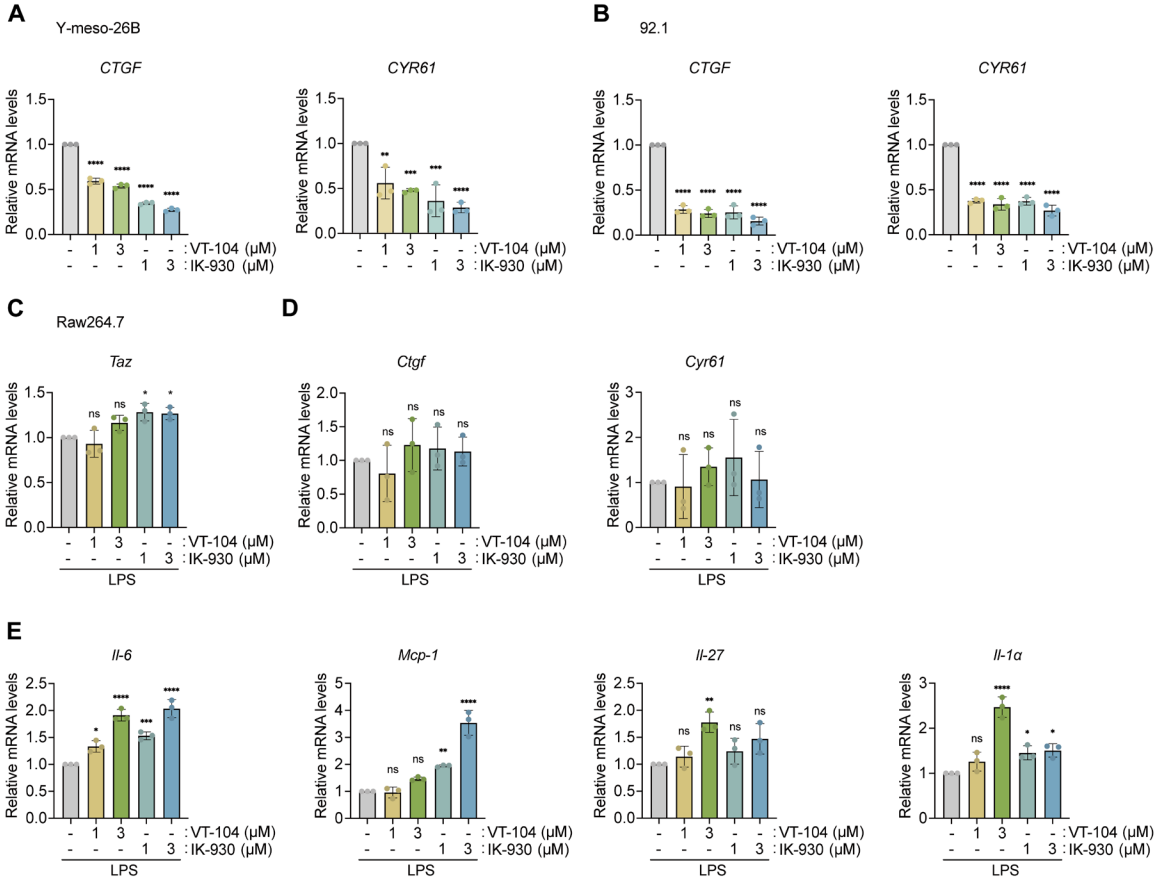

Fig. 3. TEAD inhibitors fail to affect YAP/TAZ-TEAD target genes in macrophages. (**A** and **B**) qPCR analysis of *CTGF* and *CYR61* mRNA expression levels in Y-meso-26B (A) and 92.1 (B) cells treated for 24 hours with the TEAD inhibitors VT-104 or IK-930 (1 or 3 μM). The data were analyzed by one-way ANOVA with Bonferroni tests for multiple comparisons. $^{**}P < 0.01$, $^{***}P < 0.001$, $^{****}P < 0.0001$. (**C**) qPCR analysis of TAZ mRNA expression levels in Raw264.7 cells treated with TEAD inhibitors VT-104 or IK-930 (1 or 3 μM) together with LPS (100 ng/ml) for 24 hours. The data were analyzed by one-way ANOVA with Bonferroni tests for multiple comparisons. $^{*}P < 0.05$; ns, not significant ($P > 0.05$). (**D**) qPCR analysis of *Ctgf* and *Cyr61* mRNA expression levels in Raw264.7 cells treated with TEAD inhibitors VT-104 or IK-930 (1 or 3 μM) with LPS (100 ng/ml) for 24 hours. The data were analyzed by one-way ANOVA with Bonferroni tests for multiple comparisons. ns, not significant ($P > 0.05$). (**E**) qPCR analysis of Il-6, Mcp-1, Il-27, and Il-1α mRNA expression levels in Raw264.7 cells treated with TEAD inhibitors VT-104 or IK-930 (1 or 3 μM) together with LPS (100 ng/ml) for 24 hours. The data were analyzed by one-way ANOVA with Bonferroni test for multiple comparisons. $^{*}P < 0.05$, $^{**}P < 0.01$, $^{***}P < 0.001$, $^{****}P < 0.0001$; ns, not significant ($P > 0.05$).

a strong correlation between aberrant TAZ induction and M1 but not M2 macrophage polarization. To determine whether TAZ is required for M1 or M2 polarization, we analyzed macrophage polarization in control and TAZ small interfering RNA (siRNA)–treated macrophages. Because TAZ-depleted macrophages could still be polarized into the M1 type, we conclude that TAZ induction is a consequence of M1 polarization rather than its cause (Fig. 4, C and D). This is consistent with our previous data showing that TAZ expression occurs late after iNOS expression and indicates that TAZ is a late-response gene expressed during the resolution phase of inflammation (Fig. 1K). These results suggest that TAZ may act as a downstream effector of M1 macrophage rather than an upstream regulator of M1 polarization.

To clarify the role of TAZ in M1 macrophages, we compared the LPS-induced transcriptome and cytokine secretion rates of TAZ-depleted cells with those of control cells. Unexpectedly, when we performed RNA sequencing (RNA-seq) and gene set enrichment analysis, we found that although TAZ depletion barely affected the expression of canonical TEAD target genes (Fig. 2O), it substantially altered the expression of Golgi-related genes including the regulation of protein and vesicle trafficking from the Golgi to the plasma membrane (Fig. 4, E to G). Because TAZ is localized to the Golgi in M1 macrophages, we asked whether TAZ mediates the trafficking and secretion of proinflammatory cytokines. After confirming TAZ depletion in LPS-stimulated macrophages (fig. S3A), we examined the secretion of LPS-induced cytokines. We found that culture media harvested from TAZ-depleted macrophages contained reduced levels of the proinflammatory cytokines Il-6, Mcp1, Il-27, and Il-1a (Fig. 4H). Moreover, we found that the reduced IL-6 in the culture media were accumulated in the Golgi in TAZ-depleted macrophages (Fig. 4, I and J, and fig. S3B). This reduction of inflammatory cytokine secretion indicates that TAZ depletion is associated with the resolution of inflammatory responses and suggests that TAZ is an antiresolution factor that facilitates the prolonged secretion of cytokines into inflamed tissue environment. Neither TAZ siRNA nor TEAD inhibitors affected the mRNA levels of these cytokines, confirming the transcription-independent activity of TAZ (Fig. 3E and fig. S3C). These results establish Golgi-associated TAZ as a proinflammatory factor and a critical mediator of cytokine secretion in M1 macrophages.

Next, we performed the vesicular stomatitis virus glycoprotein (VSVG)–retention using selective hooks (RUSH) secretion assay to further investigate whether TAZ affects not only cytokine secretion but also the overall proteins secretion in macrophage. In the absence of biotin, the VSVG-Streptavidin-binding peptide (SBP)–enhanced green fluorescent protein (EGFP) reporter is anchored to the endoplasmic reticulum (ER) through its interaction with streptavidin-KDEL hook. Subsequently, when biotin is added, VSVG-SBP-EGFP exits the ER, accumulates in the Golgi, and becomes subsequently secreted from the cell (Fig. 4K). In LPS-stimulated Raw264.7 cells transfected with VSVG-SBP-EGFP, depletion of TAZ led to a decrease in VSVG translocation to the plasma membrane and its retention in the Golgi after biotin treatment, compared to control group (Fig. 4, L and M). These results suggest that TAZ mediates broad range of protein trafficking at the Golgi.

The role of TLR-TAZ signaling in acute inflammatory responses

While TAZ is almost undetectable in most hematopoietic cell types (Fig. 1A), we found unexpected expression of TAZ in TLR-stimulated macrophages. To identify the signaling mechanism underlying this aberrant TAZ induction, we treated macrophages with various inhibitors of early-phase TLR signaling components that target mitogen-activated protein kinases (MAPKs) and various NF-κB signaling components (*31*, *32*). In the MAPK signaling pathway, we found inhibition of extracellular signal–regulated kinase (ERK), but not p38 or JNK, specifically blocked LPS-induced TAZ expression (Fig. 5A). Various drugs that target the common upstream components of ERK signaling have been used clinically in the treatment of various pathological conditions, such as tumorigenesis and inflammation (*40*). Thus, we tested whether treatment with MAPK kinase (MEK), B-Raf, and Ras inhibitors could recapitulate the reduction of TAZ expression induced by treatment with ERK inhibitors. While the MEK inhibitors PD0325901 and trametinib largely abolished TAZ induction (Fig. 5B), Ras and B-Raf inhibitors did not affect TAZ expression in TLR-activated macrophages (Fig. 5C and fig. S4A). Moreover, the knockdown of Raf, MEK, and ERK by siRNA revealed that down-regulation of TAZ expression occurred exclusively via MEK and ERK depletion (fig. S4, B and C). The MAPK pathway inhibitors did not, however, regulate TAZ expression in nonmacrophage cells, suggesting that the TLR-MEK-ERK-TAZ axis is a unique signaling pathway in macrophages (fig. S4, D to G). Because NF-κB and TANK-binding kinase 1 (TBK1) signaling comprise a major branch downstream of TLR signaling (*32*), we next asked whether they are involved in macrophage TAZ expression. We found pretreatment with either IKK or TBK1 inhibitors led to a substantial suppression of TAZ expression (Fig. 5, D and E). Moreover, we noticed that signaling inhibitors that suppressed TAZ induction were also associated with a blockade in IL-6 expression. Together, these results indicate that TLR stimulation leads to the early-phase activation of the MEK-ERK, IKK-p65, and TBK1 pathways, which then lead to the induction of macrophage TAZ expression (Fig. 5F).

To establish the physiologic relevance of TAZ, we generated macrophage-specific *TAZ* knockout (KO) mice by crossing $TAZ^{flox/flox}$ mice with lysozyme-Cre ($LysM^{cre}$) mice to drive Cre recombination activity in macrophages (*41*). We will refer to $TAZ^{flox/flox}$ and $LysM^{cre}$; $TAZ^{flox/flox}$ mice as control and *TAZ* knockout (*TAZ*-KO) mice, respectively. To determine *TAZ* deletion efficiency, we isolated BMDMs from control and *TAZ*-KO mice and confirmed both efficient Cre expression and *TAZ* deletion after TPA treatment (Fig. 5G). Because early-phase activation of key TLR signaling pathways induces TAZ expression, we asked whether the TLR-TAZ axis is involved in acute inflammatory responses, such as LPS-induced septic shock or dextran sulfate sodium (DSS)–induced colitis (*42*, *43*). To test this using a sepsis model, we injected control and *TAZ*-KO mice with a single intraperitoneal dose of LPS and monitored their survival for 2 days. *TAZ* deletion did not affect LPS-induced septic shock survival (Fig. 5, H and I). Next, we induced acute intestinal inflammation treating control and *TAZ*-KO mice with DSS followed by a short recovery period. Although the resulting DSS-induced colitis reduced intestinal length and body weight, we did not observe any differences between the control and *TAZ*-KO groups (Fig. 5, J and K, and fig. S2H). These in vivo results suggest macrophage TAZ is not associated with acute inflammatory responses.

The role of TAZ in tumor-associated macrophages during immune cell infiltration

It is important to note that TAZ is a late-response gene in macrophages that prolongs cytokine secretion and inflammatory responses, particularly during the resolution phase. We found that the increase

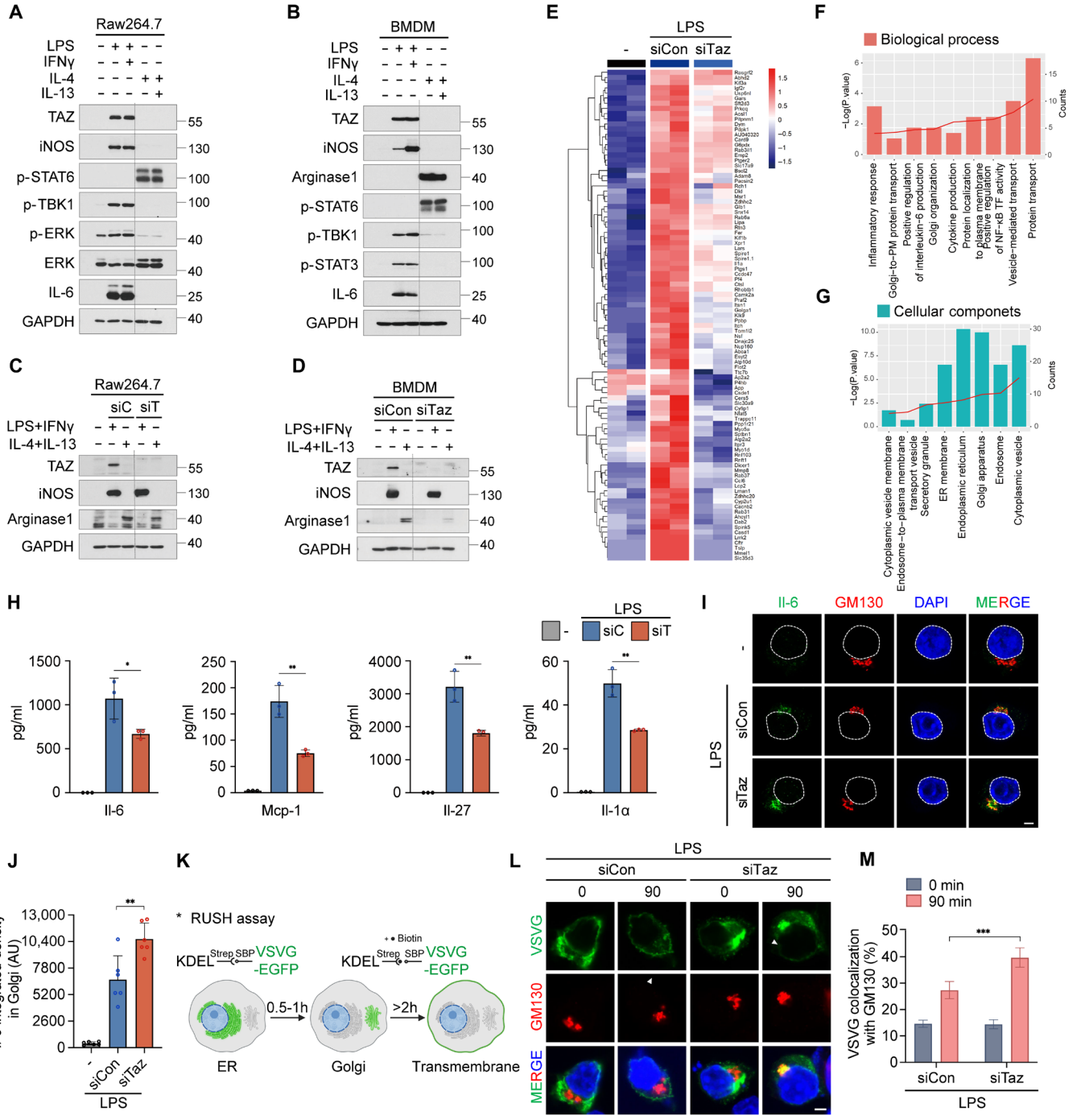

Fig. 4. Golgi-associated TAZ promotes cytokine secretion in M1 macrophages. (**A** and **B**) Immunoblotting of TAZ expression in Raw264.7 cells (A) and BMDMs (B) treated with LPS/LPS + IFN-γ or IL4/IL4 + IL13 for 24 hours. (**C** and **D**) Immunoblotting of TAZ expression in Raw264.7 cells (C) and BMDMs (D) treated with LPS/LPS + IFN-γ or IL4/IL4 + IL13 for 8 hours, followed by transfection with control or Taz siRNAs for 24 hours. (**E**) Heatmap from RNA-seq data showing gene expression changes in Raw264.7 cells stimulated with LPS and transfected with control or Taz siRNAs. (**F** and **G**) Gene ontology analysis of differentially expressed genes from (E). Database for Annotation, Visualization, and Integrated Discovery (DAVID) functional annotation revealed enrichment in biological processes (F) and cellular components (G). (**H**) Cytokine levels in Raw264.7 cells stimulated with LPS for 8 hours and then transfected with control or Taz siRNAs for 24 hours. Data were analyzed using Student's *t* tests. $^{*}P < 0.05$, $^{**}P < 0.01$. (**I**) Immunofluorescence images showing IL-6 (green) and GM130 (red) in Raw264.7 cells treated with LPS and control or Taz siRNAs for 18 hours. Scale bar, 3 μm. (**J**) Quantification of IL-6 localization in the Golgi in LPS-stimulated Raw264.7 cells. Data analyzed with Student's *t* tests, presented as means ± SEM. $^{**}P < 0.01$. (*n*): control (6), LPS + siCon (6), LPS + siTaz (7). (**K**) Schematic of the VSVG-RUSH secretion assay. (**L**) Immunofluorescence images of VSVG-SBP-EGFP in Raw264.7 cells stimulated with LPS for 20 hours and transfected with control or Taz siRNAs; visualized after biotin addition for 90 mins. Scale bar, 3 μm. (**M**) Quantification of VSVG colocalization with GM130 at different time points. Data analyzed by Student's *t* tests, presented as means ± SEM. $^{***}P < 0.001$. siCon (*n*): 0 min (20), 90 min (23); siTaz (*n*): 0 min (21), 90 min (20).

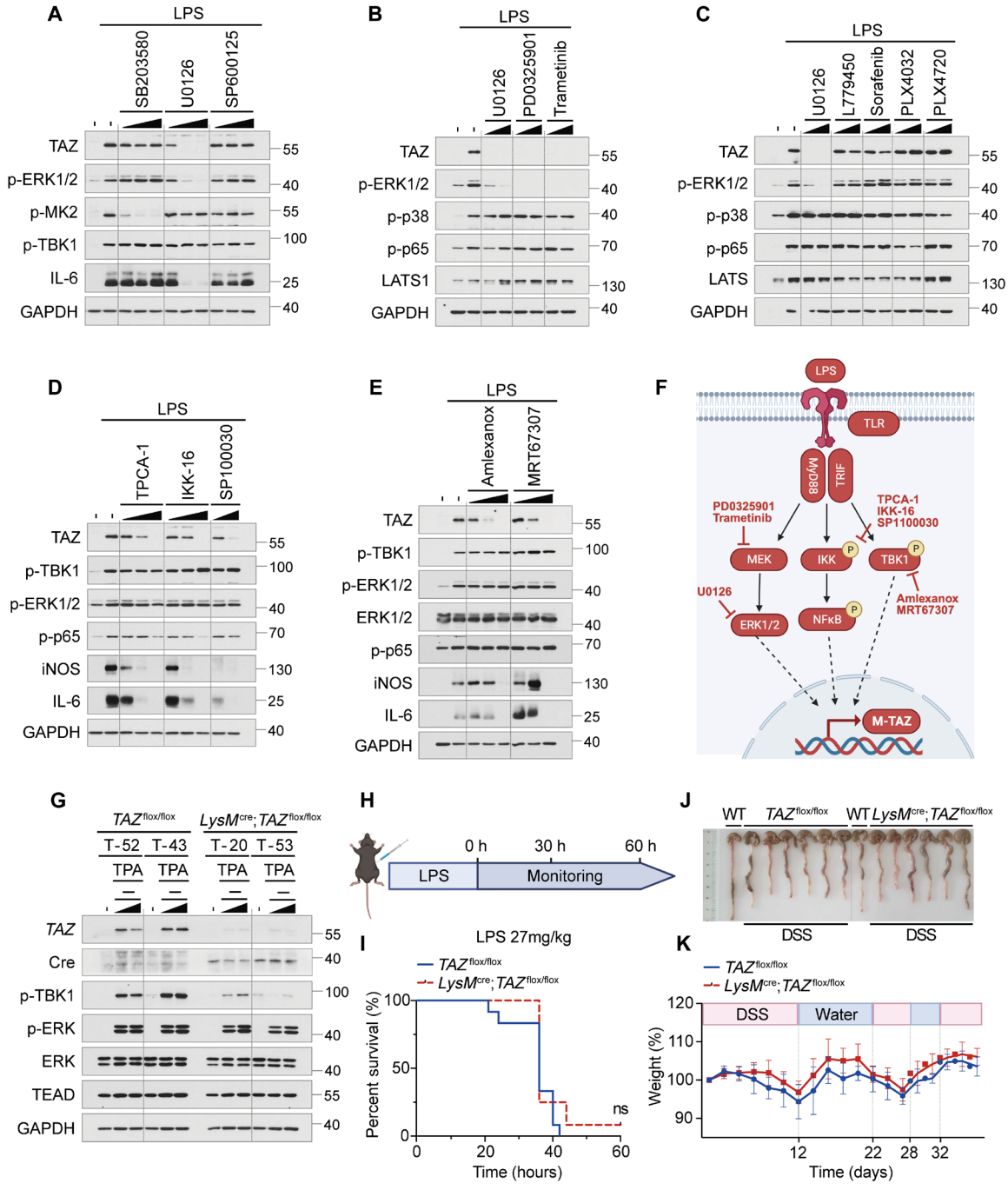

Fig. 5. The role of the TLR-TAZ signaling in acute inflammatory responses. (**A**) Immunoblotting analysis of MAPK-TAZ signaling component expression in LPS (100 ng/ml)–stimulated Raw264.7 cells after treatment with SB203580, U0126, or SP600125 (0.3, 1, or 3 μM) for 16 hours. (**B**) Immunoblotting analysis of MAPK-TAZ signaling component expression in LPS (100 ng/ml)–stimulated Raw264.7 cells after treatment with U0126 (1 or 3 μM), PD0325901 (1 or 3 μM), or trametinib (30 or 100 nM) for 16 hours. (**C**) Immunoblotting analysis of MAPK-TAZ signaling component expression in LPS (100 ng/ml)–stimulated Raw264.7 cells after treatment with U0126, L779450, sorafenib, PLX4032, or PLX4720 (1 or 3 μM) for 16 hours. (**D**) Immunoblotting analysis of NF-κB–TAZ signaling component expression in LPS (100 ng/ml)–stimulated Raw264.7 cells after treatment with TPCA-1 (0.1, 0.3, or 1 μM), IKK-16 (0.1, 0.3, or 1 μM) or SP100030 (0.1 or 0.3 μM) for 16 hours. (**E**) Immunoblotting analysis of TBK1-TAZ signaling component expression in LPS (100 ng/ml)–stimulated Raw264.7 cells after treatment with Amlexanox or MRT67307 (1, 3, or 10 μM) for 16 hours. (**F**) Schematic illustrating the signaling pathway that regulates TAZ expression in macrophages. (**G**) Immunoblotting analysis of TAZ expression in BMDMs isolated from *TAZ*$^{flox/flox}$ and *LysM*^{cre}; *TAZ*$^{flox/flox}$ mice treated with TPA (100 nM) and ionomycin (1 ug/ml) for 24 hours. (**H**) Experimental scheme illustrating the LPS septic shock model. Mice were intraperitoneally injected with LPS (27 mg/kg body weight) and monitored for 60 hours. (**I**) The survival rates of *TAZ*$^{flox/flox}$ and *LysM*^{cre}; *TAZ*$^{flox/flox}$ mice were measured for 60 hours ($n = 12$ per group). Statistics were analyzed by log-rank Mantel-Cox test. ns, not significant ($P > 0.05$). (**J**) Representative photographs of colon tissues subjected to DSS-induced colitis ($n = 6$ per group). (**K**) Experimental scheme illustrating the DSS and water treatment cycle applied to *TAZ*$^{flox/flox}$ and *LysM*^{cre}.

in TAZ expression began later than expected after TLR stimulation with LPS and that it was sustained for days (fig. S1J). This suggests a role for TAZ during the resolution phase and in chronic inflammatory responses rather than acute inflammatory responses (Fig. 5, H to K). Mechanistically, we hypothesized that this late TAZ expression may be induced in an autocrine or paracrine manner by cytokines released as part of early-phase TLR stimulation. Among the key cytokines secreted by macrophages, IL-6, and IFN-γ induced robust TAZ expression in macrophages but not nonmacrophages, even in the absence of TLR activation (Fig. 6A and fig. S5A). We further focused on the proinflammatory cytokine IL-6 because its expression and secretion were strongly correlated with TAZ induction in various contexts (Figs. 1K and 5, A, D, and E). Because the IL-6-induced increase in TAZ expression and the LPS-induced TLR-TAZ signaling activation followed a similar time course (fig. S5B), we next asked whether IL-6 receptor (IL-6R) signaling acts upstream of TAZ expression. To this end, we found inhibition of JAK and STAT3 (*44*)—key components of the IL-6 signaling pathway—abolished LPS-induced TAZ induction (Fig. 6B). This indicates that LPS-induced cytokines (phase 1) stimulate the IL6-IL6R-JAK-STAT signaling pathway to promote TAZ induction (phase 2) (Fig. 6C). With our previous results (Fig. 4, F to H), we have established TAZ as a mediator of a positive feed-forward loop that reenforces vesicular trafficking and prolongs cytokine release during chronic inflammatory responses (Fig. 6C).

The direct induction of TAZ by proinflammatory cytokines such as IL-6 explains the delay in indirect TLR-mediated TAZ expression. Furthermore, it suggests macrophage TAZ is up-regulated by secreted factors from the tumor microenvironment (TME). To test this hypothesis, we activated Raw264.7 cells to develop into tumor-associated macrophages (TAMs) by coculturing them with various cancer cell lines in trans-well cell culture chambers (fig. S5C). We found that factors secreted by human or mouse cancer cells, but not normal cells, markedly increased TAM-associated TAZ expression and activated the ERK, TBK1, and STAT signaling pathways (Fig. 6, D to F, and fig. S5D). Consistent with this result, the cancer cell–mediated TAZ induction was well correlated with iNOS expression and M1 polarization but not with M2 polarization. This suggests Golgi-associated TAZ could play proinflammatory and antitumorigenic roles in the TME.

M1-like TAMs enhance the infiltration and killing effectiveness of tumor-infiltrating lymphocytes (TILs), such as T cells and NK cells, by releasing inflammatory factors into the TME (*45*). The role of TAZ in cytokine trafficking in M1 macrophages led us to question whether it also modulates the recruitment of TILs into the TME. To test this hypothesis, we coinjected B16F10 melanoma cells together with either control or *TAZ*-depleted Raw264.7 cells subcutaneously into immunocompetent C57BL/6 mice (Fig. 6G). We found that *TAZ* depletion in M1-like TAMs impaired their antitumorigenic function and significantly enhanced melanoma growth (Fig. 6, H and I). To determine whether *TAZ* depletion affected TIL recruitment, we performed immunohistochemistry on tumor sections using CD8a and NK1.1 antibodies to quantify the degree of immune cell recruitment. We found that tumors coinjected with *TAZ*-depleted macrophages do not promote infiltration of immune cells, including cytotoxic $CD8^+$ T cells and NK cells, which likely explains the enhanced tumor growth we observed in *TAZ*-KO mice (Fig. 6, J to L). Notably, when we repeated these experiments using immunocompromised NSG mice (fig. S5E), we did not observe this difference in tumor growth. This observation further strengthens our finding that immune cell infiltration, which is facilitated by TAZ-mediated inflammatory cytokine secretion by TAMs, suppresses tumor growth (fig. S5F).

The role of macrophage TAZ in inflammation and fibrosis in chronic liver disease

We demonstrated that macrophage TAZ is not associated with acute inflammatory responses in macrophage-specific *TAZ*-KO mouse models (Fig. 5, H to K). In addition to the proinflammatory and tumor suppressive roles in TAMs, we next explored the role of macrophage TAZ in chronic liver inflammation. While previous studies implicated hepatocyte TAZ in chronic liver disease (*46*–*48*), no study explored the role of macrophage TAZ in MASH or liver fibrosis. To investigate the role of macrophage TAZ in MASH, we fed wild-type (WT) ($TAZ^{flox/flox}$) and *TAZ*-KO ($LysM^{cre}$; $TAZ^{flox/flox}$) mice a choline-deficient, L-amino acid–defined, high-fat diet (CDAHFD) diet for 34 weeks (Fig. 7A).

Prolonged exposure to CDAHFD elicits liver inflammation followed by insulin resistance, symptoms characteristic of nonalcoholic fatty liver disease (*49*). Despite body weight remaining similar in both groups following 16 weeks of CDAHFD, WT mice developed high-fat diet–induced insulin resistance, while macrophage *TAZ*-KO mice exhibited improved glucose tolerance due to enhanced insulin sensitivity (Fig. 7, B and C). Next, to measure the role of macrophage TAZ in chronic liver disease, we measured hepatic and serum markers to quantify the severity of MASH and liver fibrosis in WT and *TAZ*-KO mice after 34 weeks of exposure to CDAHFD. Compared to WT mice, the *TAZ*-KO group exhibited significantly lower blood concentrations of common serum markers for MASH, including alanine aminotransferase (ALT), triglycerides, free fatty acids, and cholesterol. These results suggest macrophage TAZ depletion protects against liver inflammation and injury (Fig. 7, D to G).

Consistent with these results, TAZ depletion also reduced the levels of fibrosis markers, such as *Mmp13*, *Timp1*, and *Col3a1* (Fig. 7H). Because macrophage TAZ is localized to the Golgi, which mediates cytokine trafficking and inflammation, we also measured the levels of various hepatic inflammatory cytokines and signaling molecules in each group. Liver specimens from *TAZ*-KO mice showed reduced levels of multiple inflammatory genes, including type 1 IFN-mediated genes (Fig. 7, I and J). Consistent with these findings, we also observed via immunohistochemistry reduced lipid droplet formation, CD8a immune cell infiltration, and liver fibrosis (Fig. 7, K to N). Together, these results establish macrophage TAZ as an antiresolution factor and suggest that it contributes to the development of MASH and hepatocirrhosis. These results demonstrate macrophage TAZ an attractive therapeutic target for preventing the progression of chronic liver disease.

DISCUSSION

In the present study, we explored the molecular mechanism in which aberrant Golgi-associated TAZ expression in M1 macrophages plays a role as a mediator of positive feed-forward loop that reenforces vesicular trafficking and prolongs cytokine release during the pathogenesis of chronic inflammation including tumorigenesis and chronic liver disease. TAZ and YAP are well-established transcriptional coactivators belonging to the TEAD family that serve as key nuclear effectors of the Hippo pathway in the context of cell proliferation, tissue regeneration, aging, and inflammation (*1*–*4*). Notably, cells in

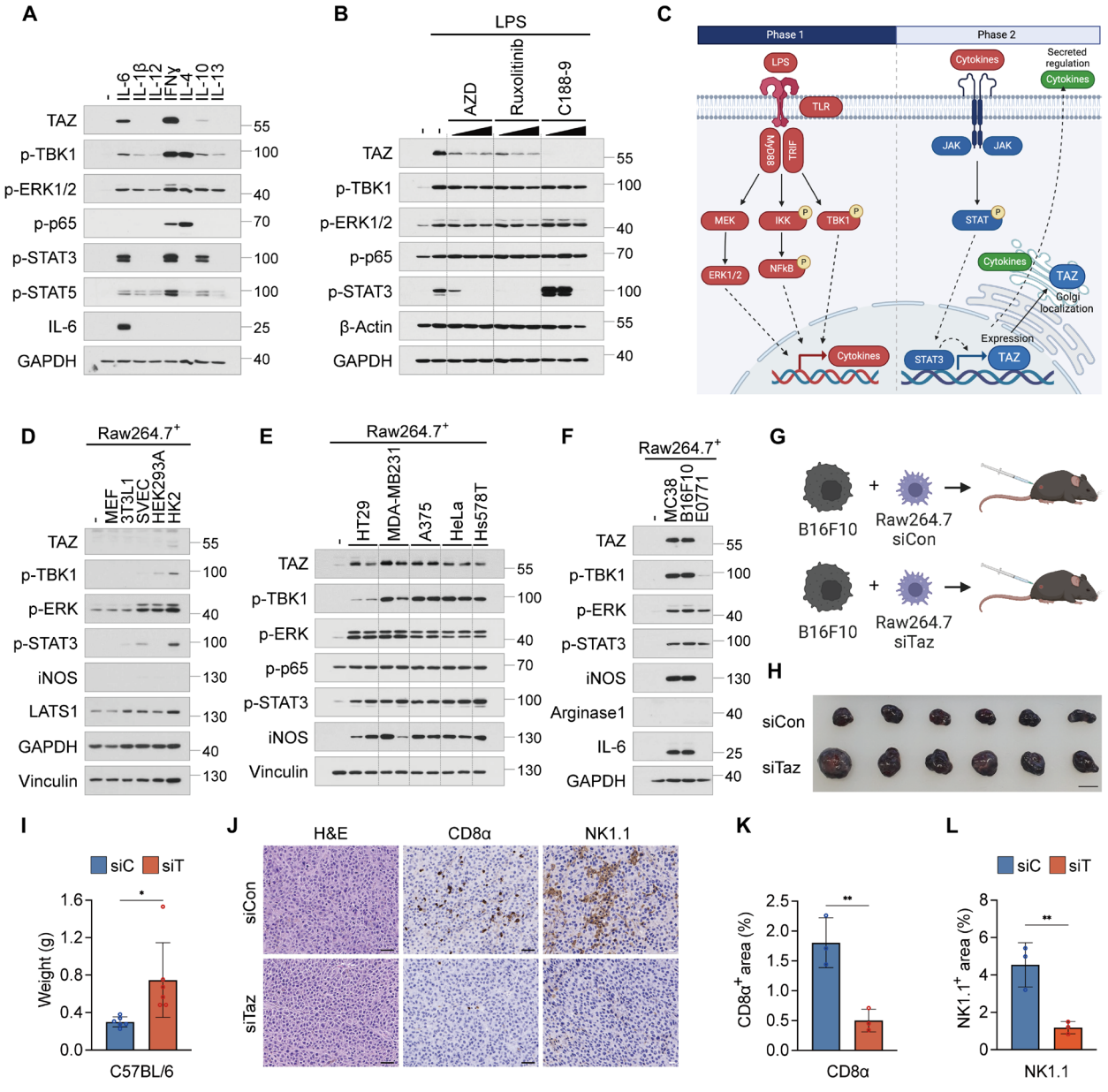

Fig. 6. The role of TAZ in tumor-associated macrophages during immune cell infiltration. (**A**) Immunoblotting analysis of TAZ expression in Raw264.7 cells treated with various cytokines, including IL-6, IL-1β, IL-12, IFN-γ, IL-4, IL-10, or IL-13 [IL-6, IL-1β, and IL-12 (100 ng/ml); IFN-γ, IL-4, IL-10, and IL-13 (20 ng/ml)] for 24 hours. (**B**) Immunoblotting of TAZ signaling components and IL-6 downstream pathway components in Raw264.7 cells treated with various doses of AZD-1486, ruxolitinib (1, 3, or 10 μM), or C188-9 (10, 20, or 30 μM) for 16 hours. (**C**) Schematic illustrating the phase 1 and 2 signaling pathways that mediate TAZ induction in macrophages. (**D**) Immunoblotting analysis of TAZ expression in Raw264.7 cells cocultured with noncancer cell lines (MEF, 3T3L1, SVEC, HEK293A, or HK2) for 24 hours. (**E**) Immunoblotting analysis of TAZ expression in Raw264.7 cells cocultured with cancer cell lines (HT29, MDA-MB-231, A375, HeLa, or Hs578T) for 24 hours. (**F**) Immunoblotting of TAZ expression in Raw264.7 cells cocultured with mouse-derived cancer cell lines (MC38, B16F10, or E0771) for 24 hours. (**G**) Schematic of allograft procedure where B16F10 cells were coinjected subcutaneously with Raw264.7/siCon or Raw264.7/siTaz into C57BL/6 mice and allowed to grow for 21 days. (**H** and **I**) Tumor images (H) and tumor weights (I) from B16F10 allografts coinjected with Raw264.7/siCon or Raw264.7/siTaz in C57BL/6 mice ($n = 6$ per group). Data were analyzed using Student's t tests, presented as means ± SD (*$P < 0.05$). Scale bar, 1 cm. (**J**) Representative histology images showing CD8+ T cells or NK cells infiltrating tumors coinjected with Raw264.7/siCon or Raw264.7/siTaz. Black scale bar, 50 μm; white scale bar, 20 μm. (**K** and **L**) Percentage of CD8+ T cells (K) or NK cells (L) infiltrating B16F10 tumors coinjected with Raw264.7/siCon or Raw264.7/siTaz. **$P < 0.01$.

the hematopoietic lineage and hematological malignancies exhibit markedly lower expression of YAP and TAZ than nonhematopoietic cells or solid tumors (*30*, *50*). Consistent with previous reports, we found that both the Raw264.7 cell line and primary isolated BMDM cells express almost undetectable levels of TAZ and YAP under basal conditions. TAZ levels rise markedly, however, only later upon macrophage activation. After LPS-mediated TLR activation, we observed a late but significant increase in the mRNA and protein levels of TAZ, but not of YAP. In addition, the increase in active markers in the intron region of Wwtr1 (TAZ) suggests that there may be an intronic enhancer. Although we found the delayed time course of TAZ induction was clearly distinct from that of the early-response signaling

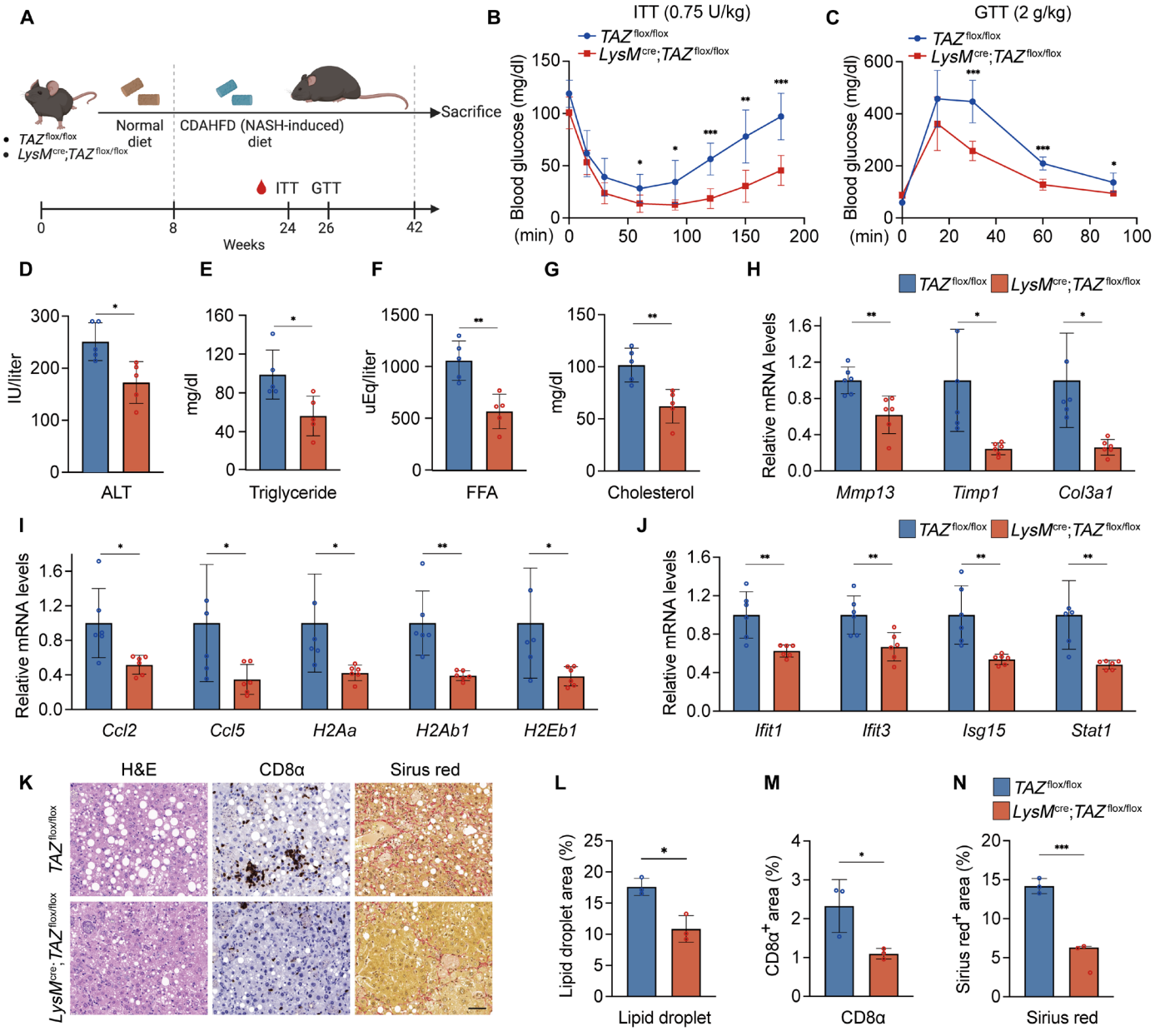

Fig. 7. Role of macrophage TAZ in the inflammation and fibrosis of chronic liver disease. (**A**) Experimental scheme for the CDAHFD-induced MASH model. The MASH model was generated by feeding *TAZ*$^{flox/flox}$ and *LysM*^{cre}; *TAZ*$^{flox/flox}$ mice groups with CDAHFD for 34 weeks. ITT, insulin tolerance test; GTT, glucose tolerance test. (**B** and **C**) Insulin tolerance tests (B) and glucose tolerance tests (C) were performed on *TAZ*$^{flox/flox}$ and *LysM*^{cre}; *TAZ*$^{flox/flox}$ groups after 16 or 18 weeks of CDAHFD, respectively. Blood glucose was measured at the indicated time points after insulin or glucose injection. $n = 4$ independent animals. (**D** to **G**) Serum levels of ALT (D), triglycerides (E), free fatty acids (F) and cholesterol (G) were measured in both groups after 34 weeks of CDAHFD. $n = 5$ independent animals. Data were analyzed using Student's *t* tests and presented as means ± SD. $^*P < 0.05$, $^{**}P < 0.01$. (**H**) qPCR analysis of hepatic *Mmp13*, *Timp1*, and *Col3a1* mRNA expression after 34 weeks of CDAHFD in both groups. $n = 6$. Data were analyzed using Student's *t* tests. $^*P < 0.05$, $^{**}P < 0.01$. (**I**) qPCR analysis of hepatic *Ccl2*, *Ccl5*, *H2Aa*, *H2Ab1*, and *H2Eb1* mRNA expression in the *TAZ*$^{flox/flox}$ and *LysM*^{cre}; *TAZ*$^{flox/flox}$ groups after 34 weeks of CDAHFD. $n = 5$ independent animals. $^*P < 0.05$, $^{**}P < 0.01$. (**J**) qPCR analysis of hepatic *Iit1*, *Ifit3*, *Isg15*, and *Stat1* mRNA expression after 34 weeks. $n = 6$. $^{**}P < 0.01$. (**K**) Representative histology images of CD8$^+$ T cells or Sirius red staining in liver tissue harvested from *TAZ*$^{flox/flox}$ and *LysM*^{cre}; *TAZ*$^{flox/flox}$ mice. Scale bar, 50 μm. (**L** to **N**) Percentage of lipid droplets (L), CD8$^+$ T cells (M), and Sirius red (N) in liver tissue from both groups after 34 weeks. $n = 3$ independent animals. Data were analyzed using Student's *t* tests. $^*P < 0.05$, $^{***}P < 0.001$.

pathways (phase 1), such as MEK-ERK and IKK-p65, the inhibition of these pathways abolished TAZ induction. This suggested TAZ expression is continuous from and dependent on the early activation of TLR signaling. We further found that direct stimulation of JAK-STAT signaling by TLR signaling-induced cytokines (phase 2), such as IL-6 and IFN-γ, can induce TAZ expression. STAT3 is known as a transcription factor that suppresses the resolution phase, leading to chronic disease and tumor formation (*51*, *52*). Treatment with STAT3 inhibitor substantially reduced TAZ expression suggesting that STAT3 may act as the transcription factor for TAZ. Whether STAT3 directly induces TAZ expression warrants further investigation. The delayed and prolonged nature of this TAZ expression response

led us to hypothesize that a dysregulation of TAZ expression may perturb inflammation resolution and the restoration of tissue homeostasis. This would affect the link from acute inflammatory responses to persistent chronic inflammation and innate immune responses to adaptive immunity. Consistent with this hypothesis, we found TAZ modulates the secretion of cytokines in the late phase of inflammatory responses, suggesting that TAZ acts as an antiresolution factor during the pathogenesis of chronic inflammation.

Recent studies on macrophage repolarization between the M1 and M2 subtypes have provided insight into novel strategies for treating inflammatory diseases (*18*, *26*). TAZ expression is specifically linked to M1 macrophage polarization and induced by various stimuli, such as LPS, cytokines, *E. coli*, and cancer cell–conditioned media. We found a tight correlation between the expression of TAZ and M1 but not M2 markers in various physiologic and pathologic conditions. TAZ expression, rather than being a prerequisite for M1 polarization, acts instead as a critical mediator of the proinflammatory and antitumorigenic functions of M1 macrophages during chronic inflammation and tumorigenesis. M1 macrophages secrete various proinflammatory cytokines and chemokines, such as TNF-α, IL-6, and IL-1α/β (*18*, *26*), which subsequently help recruit T cells and NK cells to the TME and to sites of infection or injury (*45*, *53*). Unexpectedly, we have established TAZ as an undescribed Golgi-associated protein in M1-polarized macrophages, which facilitates their secretion of proinflammatory cytokines, thereby maintaining and promoting macrophage-mediated immune regulation. We have demonstrated that TAZ depletion decreased cytokine secretion and suppressed immune cell infiltration, thereby reducing the antitumorigenic function of M1-type TAM in tumor growth and the proinflammatory function of monocyte-derived hepatic macrophages in high-fat diet–associated liver disease.

In this study, we performed several experiments to establish TAZ as a Golgi-associated protein in activated macrophages. In the process, we unveiled unprecedented implications and therapeutic strategies for exploiting TAZ as a target for the treatment of chronic inflammatory diseases. Our results also included several critical discrepancies with previous reports related to the role of TAZ and YAP in macrophages. Although there was some existing controversy regarding the basal expression levels, induction rates, and involvement of TAZ and YAP in macrophages undergoing M1/M2 polarization, all previous studies consistently suggested a role for TAZ and YAP in macrophages acting as (i) nuclear effectors of the Hippo pathway and (ii) transcriptional coactivators of TEAD, inducing the expression of its target genes to regulate immune cell function and inflammation (*8*–*12*, *14*). Consistent with data available in public databases, our results clearly demonstrated almost undetectable expression of TAZ and YAP in unstimulated macrophages. We found it is only the expression of TAZ, not YAP, that rises significantly in M1 macrophages late after LPS or cytokine stimulation. Although TAZ expression was not a prerequisite for M1 polarization, TAZ-mediated cytokine secretion was critical for conferring the proinflammatory and antitumorigenic traits characteristic of M1 macrophages. We were surprised to find through multiple biochemical assays an atypical localization of TAZ at the Golgi compartment of activated macrophages. Fractionation assays, sucrose density gradient assays, and immunofluorescence assays with multiple antibodies against TAZ, YAP, and other subcellular markers consistently showed expression of TAZ exclusively at the Golgi compartment. In our hands, we did not detect significant YAP expression in macrophages. Notably, activated macrophages showed nearly undetectable levels of YAP and a diffuse cytoplasmic localization of TEAD. Here, we provide a reference that demonstrates the role of Hippo-independent Golgi-associated TAZ in macrophage activation. Macrophage TAZ did not show Hippo kinase LATS1/2-induced phosphorylation or nucleocytoplasmic translocation. Moreover, Golgi-associated TAZ and cytoplasmic TEAD did not form a transcriptional complex in the nucleus in response to conditions that typically stimulate the Hippo pathway or activate macrophages. Until now, the main regulatory mechanism for TAZ was nuclear-cytoplasmic translocation via Hippo-mediated phosphorylation (*1*–*4*, *33*). Thus, the unexpected finding that TAZ in macrophages is associated with the Golgi and independent of Hippo/TEAD pathway suggested that it may also have a distinct function in inflammation. Consistent with its Golgi localization, we found evidence via a transcriptome analysis and cytokine assessment of TAZ-depleted activated macrophages that TAZ modulates LPS-induced Golgi-related gene expression and proinflammatory cytokine secretion. We speculate that depletion of Golgi-associated TAZ could lead to changes in gene expression via secondary effect due to Golgi dysfunction. Previous studies suggest that Golgi-resident proteins could indirectly affect Golgi-related target genes. For instance, studies have shown that depletion of Golgi-associated proteins such as giantin, Golgin-97, and GP97 could induce changes in gene expression upon Golgi dysregulation (*54*–*56*). In line with previous studies, mechanisms that govern the indirect regulation of Golgi-related target gene expression via TAZ warrants further investigation.

To further show whether TAZ affects broader range of protein secretion in addition to cytokines, we conducted VSVG-RUSH assay. Our results show that TAZ likely regulates the overall secretion of proteins, suggesting that the role of TAZ is not limited to specific cargo. Because vesicular transport includes both the sorting and formation stages, TAZ is more likely to regulate vesicle formation, thereby affecting the overall secretion process rather than selecting specific cargo.

Small-molecule TEAD inhibitors that suppress TEAD palmitoylation and dissociate YAP/TAZ-TEAD protein-protein interactions in YAP/TAZ-driven solid tumor cells are being intensively developed as anticancer therapeutics (*27*–*29*). Although these TEAD inhibitors might also be useful for modulating the function of macrophages in the context of treating inflammatory diseases (*12*, *13*), our results indicate that neither TEAD nor TAZ are present in the nucleus and do not bind to one another in macrophages. This suggests that current pharmacological strategies for blocking TAZ-TEAD interaction and transcriptional activity will prove ineffective in macrophages. Consistent with this, we demonstrate that, although TEAD inhibitors currently being tested in clinical trials suppressed YAP/TAZ-TEAD target genes in solid tumor cells (*37*, *38*), they were ineffective in macrophages. Thus, predicting the outcome of TAZ inhibition and achieving proper control of these processes will require a careful tissue and cell type–specific clarification of the underlying mechanisms to target macrophage TAZ. Although few studies have observed cytoplasmic localization of TEAD in cancer cells (*35*), our results provide evidence demonstrating an atypical localization of cytoplasmic TEAD and Golgi-associated TAZ in activated macrophages. In contrast to previous reports, we were unable to observe any Hippo pathway–dependent nucleocytoplasmic translocation of Golgi-associated TAZ. Going forward, the interacting partners and signaling pathways that govern macrophage TAZ will likely present

unexplored therapeutic targets for the treatment of chronic inflammatory diseases and tumorigenesis.

METHODS

Public data analysis

TAZ/YAP transcript expression data were obtained from the Human Protein Atlas database in the form of matrices containing normalized transcripts per million (nTPM) values. The calculation of *P* values was carried out using Prism 9.

Mice

Myeloid cell–specific *TAZ*-KO mice were generated by crossing *LysM*$^{cre/+}$ transgenic mice with *TAZ*$^{flox/flox}$ mice (*41*). The resulting *LysM*$^{cre/+}$; *TAZ*$^{flox/+}$ offspring were then backcrossed to the *TAZ*$^{flox/flox}$ strain to obtain *LysM*$^{cre/+}$; *TAZ*$^{flox/flox}$ (*TAZ*-KO) mice. We used *TAZ*$^{flox/flox}$ mice as controls. *TAZ* floxed mice were genotyped as previously explained. Nonobese diabetic/severe combined immunodeficient (NOD/SCID) mice and WT C57BL/6 J mice were purchased from JaBio (South Korea). These mice were bred in a specific pathogen–free (SPF) facility in the Yonsei Laboratory Animal Research Center. They were fed a normal chow diet (PicoLab Rodent Diet 20, Orient Bio Inc.) and maintained under a 12-hour light-dark cycle in the SPF facility at 23°C and 40 to 60% humidity. All the animal experiment protocols were conducted under guidelines approved by the Institutional Animal Care and Use Committee at the Yonsei University (documentation no. 201906-922-03).

Cell culture

All cell lines were maintained at 37°C under 5% CO_2. The Raw264.7 cell line was purchased from the American Type Culture Collection. The Raw264.7, MEF, human embryonic kidney (HEK) 293T, HEK293A, HaCaT, SVEC, iBMDM, BV2, Hs578T, E0771, 3T3L1, HK2, HT29, A375, HeLa, MC38, and B16F10 cell lines were cultured in Dulbecco's modified Eagle's medium (DMEM) (Hyclone, SH30022.01) containing 10% fetal bovine serum (FBS) (Gibco, 16000-044) and 1% penicillin/streptomycin (Gibco, 15140-122). The MDA-MB-231, Y-meso-26B, and 92.1 cell lines were cultured in RPMI (Hyclone, SH30027.01) containing 10% FBS (Gibco, 16000-044) and 1% penicillin/streptomycin (Gibco, 15140-122).

Isolation of BMDMs

Bone marrow cells were harvested from femurs and tibias of WT, *TAZ*$^{flox/flox}$ and *LysM*$^{cre/+}$; *TAZ*$^{flox/flox}$ mice and differentiated in differentiation medium [DMEM containing 10% FBS, 1% penicillin/streptomycin, and macrophage colony-stimulating factor (30 ng/ml; PeproTech, 315-02)]. On day 3, an additional 15 ml of differentiation medium was added. On day 6, all the media were replaced with fresh differentiation medium. After 7 days, BMDMs were seeded (6×10^5) in six-well nontissue culture plates using culture medium (DMEM containing 10% FBS and 1% penicillin/streptomycin).

Isolation of human monocytes using leukocyte reduction system chambers and macrophage culture

Peripheral blood mononuclear cells (PBMC) were isolated through density centrifugation using Histopaque (Sigma-Aldrich) taken from leukocyte reduction system chambers provided by the Korean Red Cross. Following the manufacturer's instructions, human CD14 magnetic beads and MACS cell separation columns (Miltenyi Biotec) were used to purify the monocyte population from the PBMCs. Purified monocytes were plated in 12-well tissue culture plates at a density of 5×10^5 cells/ml and allowed to grow for 6 days in RPMI supplemented with 10% FBS, penicillin (100 U/ml), streptomycin (100 mg/ml), and human granulocyte-macrophage colony-stimulating factor (50 ng/ml; PeproTech). Half the medium was removed and replenished with fresh media on day 3 and the adherent cells were collected on day 6 using a scraper. Our usage of human blood cells provided by the Korean Red Cross was approved by the Institutional Review Board of Yonsei University (permit no.: 7001988-202301-BR-1366-02).

Coculture of macrophage cells with cancer cells or normal cells

Raw264.7 cells were seeded in 12-well plates at a density of 1.5×10^5 cells. The cancer cells (HT29, MDA-MB231, A375, HeLa, Hs578T, MC38, B16F10, or E0771) or normal cells (MEF, 3T3L1, SVEC, HEK293A, and HK2) were cocultured in a 12-well transparent PET membrane 1.0 μm (Falcon, 353103) insert with the Raw264.7 cells at a 1:1 ratio. After incubation for 24 hours, the trans-well inserts were discarded, and the Raw264.7 cells were collected to examine their TAZ expression through immunoblotting analysis.

Chemical agents

The following chemical agents were used in this study: LPS (Invivogen, tlrl-eblps), Poly(I:C) (Invivogen, tlrl-pic), Pam3CSK4 (Invivogen, tlrl-pms), TPA (Sigma-Aldrich, P1585), 5p-dsRNA (Invivogen, tlrl-3prna), 3p-hpRNA (Invivogen, tlrl-hprna), Poly(dA:dT) (Invivogen, tlrl-patn), ionomycin (Sigma-Aldrich, I0634), IFN-γ (PeproTech, 315-05), simvastatin (Sigma-Aldrich, S6196), latrunculin B (Sigma-Aldrich, L5288), VT-104, IK-930, IL-4 (PeproTech, 214-14), IL-13 (PeproTech, 210-13), SB203580 (Selleckchem, S1076), U0126 (Selleckchem, S1102), SP600125 (Selleckchem, S1460), PD0325901 (Selleckchem, S1036), trametinib (Selleckchem, S2673), L779450 (Selleckchem, S6680), sorafenib (Selleckchem, S7397), PLX4032 (Selleckchem, S1267), PLX4720 (Selleckchem, S1152), sotorasib (MedChemExpress, HY-114277), RMC-7977 (MedChemExpress, HY-156498), TPCA-1 (Selleckchem, S2824), IKK-16 (Selleckchem, S2882), SP100030 (MedChemExpress, HY-110177), Amlexanox (Selleckchem, S3648), MRT67307 (Selleckchem, S7648), IL-1β (PeproTech, 211-11B), IL-12 (PeproTech, 210-12), IL-10 (PeproTech, 210-10), and AZD-1480 (Selleckchem, S2162), ruxolitinib (Selleckchem, S1378), and C188-9 (Selleckchem, S8605).

Bacterial strain and macrophage treatment

The *E. coli* strain DH5α (ECOS, ITY-YE607) was used for macrophage stimulation. Raw264.7 cells were treated with *E. coli* [2×10^6 colony-forming units (CFU)/ml and 6×10^6 CFU/ml] for 16 hours.

Immunoblotting analysis

Immunoblotting was performed using a standard protocol. Phos-tag reagents were purchased from Wako Chemicals (AAL-107), and gels with phos-tag were prepared according to the manufacturer's guidelines. Protein samples were loaded onto the wells of a 9% SDS–polyacrylamide gel electrophoresis gel and transferred to polyvinylidene fluoride membranes (Millipore). Membranes were blocked with 5% skim milk in tris-buffered saline containing 0.2% Tween (TBS-T) for 1 hour at room temperature. Then, they were incubated with primary antibodies overnight at 4°C with gentle agitation. The membranes were washed three times with TBS-T buffer and incubated with the appropriate horseradish peroxidase–linked

immunoglobulin G (IgG) secondary antibody in skim milk for 1 hour. After the membranes were washed four times, they were exposed to x-ray film for development.

Immunofluorescence microscopy

Coverslips were prepared for cell seeding by pretreating them with a 1:20 diluted solution of poly-L-ornithine (Sigma-Aldrich, P4957) at 37°C for 15 min, followed by a quick wash with phosphate-buffered saline (PBS) (WellGene, LB001-02). Cells were seeded onto 12-well plates on coverslips. Cells were fixed in 4% paraformaldehyde (Thermo Fisher Scientific, 28908) in PBS for 20 min and permeabilized with 0.1% Triton X-100/PBS for 10 min. After blocking with 3% bovine serum albumin (BSA)/PBS for 30 min, they were incubated overnight at 4°C in primary antibodies diluted in 3% BSA/PBS. Then, the coverslips were incubated with secondary antibodies diluted in 3% BSA/PBS for 2 hours. The slides were mounted with Prolong gold antifade reagent containing 4′,6-diamidino-2-phenylindole (Invitrogen, P36930). Image acquisition was performed using a confocal microscope (Leica Microsystems, SP8).

RUSH assay

Raw264.7 cells were cultured on glass coverslips and treated with LPS and siRNA. The cells were then transfected with Str-Ii_VSVG-SBP-EGFP (Addgene, no. 65300) using the PEI-Macrophage transfection reagent (Polyplus, no. 103-05 N). After 19 hours, the cells were treated with 40 μM biotin and fixed with 4% paraformaldehyde at 0 and 90 min. GM130 immunofluorescence staining was performed, and images were acquired using a Leica SP5 confocal laser scanning microscope with a 63× oil objective and 12× zoom. The degree of signal overlap between the GM130 and VSVG-EGFP channels was analyzed using Pearson's correlation coefficient in Leica LAS X software.

Immunoprecipitation assay

Cells were washed once with PBS and lysed in ice-cold lysis buffer (0.15 M NaCl, 0.05 M tris-HCl, and 0.5% Triton X-100) with one tablet each of EDTA-free protease/phosphatase inhibitor cocktail (Thermo Fisher Scientific, 78446). For immunoprecipitations, magnetic beads (Bio-Rad, 1614023) and nTAZR1 antibody were added to the lysates and incubated with rotation overnight at 4°C. The samples were washed four times with lysis buffer. Immunoprecipitated proteins were denatured by the addition of 2× sample buffer and boiled for 8 min. Then, the samples were analyzed by immunoblotting analysis.

Organelle fractionation

To examine the intracellular localization of TAZ induced by LPS treatment, organelles were isolated from RAW264.7 cells using sucrose gradient centrifugation. In brief, cells cultured in three 150-mm culture dishes were harvested using a cell scraper. After centrifugation at 3000 rpm for 10 min, the pellets were resuspended in 1.5 ml of cold ST buffer [250 mM sucrose and 10 mM tris-HCl (pH 7.3)] and lysed using a ball bearing homogenizer with a 22-μm ball. The resulting cell lysates were mixed with 62% sucrose buffer [804.9 mg of sucrose in 1 ml of 10 mM tris-HCl (pH 7.4)] to reduce the sucrose concentration to 38%. The samples were loaded at the bottom of sucrose layers of 35% and 28%. After ultracentrifugation at 200,000*g* for 24 hours using a SW41Ti swinging bucket rotor, fractions were collected and examined using Western blotting. Antibodies against GM130 and giantin were used to identify the Golgi membrane. Cellubrevin was used to identify endosomal compartments.

Antibodies

The following antibodies were used for immunoblotting analysis, immunofluorescence microscopy, immunoprecipitation assays, and immunohistochemistry: YAP [Cell Signaling Technology (CST), no. 14074; Santa Cruz Biotechnology, sc-101199), TAZ (CST, no. 4883; NOVUS, NB600-220; Abcam, ab119373; nTAZR1), pan-TEAD (CST, no. 13295), TEAD4 (Santa Cruz Biotechnology, sc-101184), LATS (CST, no. 9153), ERK1/2 (CST, no. 4377), p-ERK1/2 (CST, no. 4695), p-p38 MAPK (CST, no. 8690), p-MK2 (CST, no. 3316), p65 (CST, no. 8242), p-p65 (CST, no. 3033), p-STAT3 (CST, no. 9145), p-STAT5 (CST, no. 9351), p-STAT6 (CST, no. 56554), TBK1 (CST, no. 38066), p-TBK1 (CST, no. 5483), IL-6 (CST, no. 12912), IL-1β (CST, no. 12242), TNF-α (CST, no. 11948), iNOS (CST, no. 13120), arginase-1 (CST, no. 93668), GM130 (BD, 610822), lamin A/C (CST, no. 4777), TGN38 (Bio-Rad, AHP449G), β-actin (Santa Cruz Biotechnology, sc-47778), giantin (abcam, ab80864), cellubrevin (abcam, ab5789), Cre (CST, no. 15036), vinculin (Santa Cruz Biotechnology, sc-7364), glyceraldehyde-3-phosphate dehydrogenase (Santa Cruz Biotechnology, sc-25778), CD8α (CST, no. 98941), NK1.1 (Invitrogen, no. MA1-70100), and H3K27ac antibody (catalog no. 4729, Abcam).

RNA extraction, cDNA synthesis, and quantitative real-time polymerase chain reaction

Cells were harvested for RNA extraction using the RNeasy Plus mini kit (Qiagen, 74136). Subsequently, the resulting RNA samples were reverse transcribed to complementary DNA (cDNA) using iScript reverse transcriptase (Bio-Rad, 1708890). Quantitative real-time polymerase chain reaction (qRT-PCR) was performed using the KAPA SYBR FAST qPCR Master Mix (2X) (Kapa Biosystems, KK4605) and the 7300 real-time PCR system (Applied Biosystem). Primer pair sequences were as follows: Wwtr1 (Taz), 5′-GTCACCAACAGTAGCTCAGATC-3′ (forward) and 5′-AGTGATTACAGCCAGGTTAGAAAG-3′ (reverse); Yap, 5′-ACCCTCGTTTTGCCATGAAC-3′ (forward) and 5′-TGTGCTGGGATTGATATTCCGTA-3′ (reverse); Il-6, 5′-ACCAGAGGAAATTTTCAATAGGC-3′ (forward) and 5′-TGATGCACTTGCAGAAAACA-3′ (reverse); Gapdh, 5′-GCCTGGAGAAACCTGCCAAGTATG-3′ (forward) and 5′-GAGTGGGAGTTGCTGTTGAAGTCG-3′ (reverse); CYR61, 5′-AGCCTCGCATCCTATACAACC-3′ (forward) and 5′-TTCTTTCACAAGGCGGCACTC-3′ (reverse); CTGF, 5′-TTAGAGCCAACTGCCTGGTC-3′ (forward) and 5′-GCGTTGTCATTGGTAACCCG-3′ (reverse); Cyr61, 5′-GCACCTCGAGAGAAGGACAC-3′ (forward) and 5′-CAAACCCACTCTTCACAGCA-3′ (reverse); Ctgf, 5′-CAAGGACCGCACAGCAGTT-3′ (forward) and 5′-AGAACAGGCGCTCCACTCTG-3′ (reverse); Mcp-1, 5′-TTAAAAACCTGGATCGGAACCAA-3′ (forward) and 5′-GCATTAGCTTCAGATTTACGGGT-3′ (reverse); Il-27, 5′-CTCTGCTTCCTCGCTACCAC-3′ (forward) and 5′-AGGGGCAGCTTCTTTTCTTC-3′ (reverse); Il-1α, 5′-ACGAAGACTACAGTTCTGCCA-3′ (forward) and 5′-CTTCCCGTTGCTTGACGTTG-3′ (reverse); Mmp13, 5′-TGCTTCCTGATGATGACGTTCAAGG-3′ (forward) and 5′-TGGGATGCTTAGGGTTGGGGTC-3′ (reverse); Timp1, 5′-CTCAAAGACCTATAGTGCTGGC-3′ (forward) and 5′-CAAAGTGACGGCTCTGGTAG-3′ (reverse); Col3a1, 5′-CTGTAACATGGAAACTGGGGAAA-3′ (forward) and 5′-CCATAGCTGAACTGAAAACCACC-3′ (reverse); Ccl2, 5′-AGGTCCCTGTCATGCTTCTG-3′

(forward) and 5′-TCTGGACCCATTCCTTCTTG-3′ (reverse); Ccl5, 5′-TGCCCACGTCAAGGAGTATTT-3′ (forward) and 5′-TTCTCTGGGTTGGCACACACT-3′ (reverse); H2Ab1, 5′-AGCCCCATCACTGTGGAGT-3′ (forward) and 5′-GATGCCGCTCAACATCTTGC-3′ (reverse); H2Eb1, 5′-GCGGAGAGTTGAGCCTACG-3′ (forward) and 5′-CCAGGAGGTTGTGGTGTTCC-3′ (reverse); Ifit1, 5′-CTGAGATGTCACTTCACATGGAA-3′ (forward) and 5′-GTGCATCCCCAATGGGTTCT-3′ (reverse); Ifit3, 5′-TCAGGCTTACGTTGACAAGGT-3′ (forward) and 5′-CACACTTTAGGCGTGTCCATC-3′ (reverse); Isg15, 5′-GGTGTCCGTGACTAACTCCAT-3′ (forward) and 5′-TGGAAAGGGTAAGACCGTCCT-3′ (reverse); Stat1, 5′-ACAGCTGCTGCTCCACAAGA-3′ (forward) and 5′-CTGAGTGAGCTCGATGGAATTCA-3′ (reverse); Erk, 5′-GGTTGTTCCCAAATGCTGACT-3′ (forward) and 5′-CAACTTCAATCCTCTTGTGAGGG-3′ (reverse); Mek, 5′-AAGGTGGGGGAACTGAAGGAT-3′ (forward) and 5′-CGGATTGCGGGTTTGATCTC-3′ (reverse); and Braf, 5′-TGATGCGCTGTCTTCGGAAAT-3′ (forward) and 5′-GCCAGGCTCAAAATCAAACACT-3′.

siRNA transfection

BMDM and Raw264.7 cells were transfected [100 μl of Opti-MEM medium (Thermo Fisher Scientific, no. 31985070), 12 μl RNAi Max (Invitrogen, 13778150), and 4 μl of 10 μM siRNA] for 30 hours. The siRNAs used were as follows: control siRNA (Dharmacon siGENOME nontargeting control pool D-001206-13-20), siWwtr1 (Dharmacon siGENOME SMARTPool no. M-041057-01-0010), B-raf siRNA (Dharmacon siGENOME SMARTPool no. M-040325-01-0005), Mek siRNA (Dharmacon siGENOME SMARTPool no. M-040605-01-0005), and Erk siRNA (Dharmacon siGENOME SMARTPool no. M-040613-01-0005).

RNA-seq analysis

Total RNA was isolated from RAW-control, RAW-siCon, and RAW-siTaz cell lines. CLC Genomics Workbench 9.5.3 software (Qiagen, Germany) was used to map the reads to the mouse genome (mm10, build name GRCm38) and generate gene expression values in the form of nTPM. All bioinformatic analyses were performed with R v.4.1.2. Hierarchical clustering of these data was performed with the R package Pheatmap (version 1.0.12). Differentially expressed genes with opposite expression patterns for siCon and siTaz samples compared to control were selected if they showed an absolute fold change >2 and a P value <0.05 as measured with Gaussian T-tests. Gene Ontology enrichment analysis was performed with P values <0.05 (Benjamini-Hochberg corrected) considered statistically significant.

Chromatin immunoprecipitation assay and chromatin immunoprecipitation sequencing

A total of 5×10^6 trypsinized Raw264.7 cells were cross-linked for 15 min with 1% formaldehyde, quenched in 0.125 M glycine for 10 min, and washed with PBS. Cell pellets were lysed with cell lysis buffer, and their nuclei were isolated by centrifugation at 7400 rpm for 30 s. The pellets were gently resuspended in nuclei lysis buffer and sonicated for 10 cycles (30 s on/30 s off). The supernatants were incubated for 1 hour with 10 μg of rabbit IgG and 10 μl of Protein A magnetic beads (catalog no. 10001, Invitrogen) for preclearing. Immunoprecipitation was conducted with precleared chromatin, 1 μg of the H3K27ac antibody (catalog no. 4729, Abcam), and 10 μl of Protein A magnetic beads overnight at 4°C on a rotator. The next day, the immunocomplexes were washed once with IP Wash I Buffer, twice with high-salt buffer, once with IP Wash II buffer, and twice with TE (pH 8.0). The washed immunocomplexes were then eluted with 200 μl of elution buffer for 30 min at 45°C in a thermomixer at 1000 rpm. The eluate was de–cross-linked with ribonuclease A (1 μg/μl) and 0.25 M NaCl overnight in a 65°C water bath. The next day, after a 2-hour incubation with Proteinase K (catalog no. P8107, NEB), the immunoprecipitated DNA was purified using a QIAquick PCR purification kit (catalog no. 28106, QIAGEN) and eluted in 50 μl of elution buffer. For chromatin immunoprecipitation sequencing (ChIP-seq) library construction, 40 μl of purified ChIP DNA was added to a NEXTflex ChIP-seq kit (catalog no. NOVA-5143-02, PerkinElmer), and the protocol was performed according to the manufacturer's instructions. Fifteen PCR cycles were used for final library amplification, and the quality of each ChIP-seq library was assessed via Bioanalyzer using the High Sensitivity chip (Agilent). The average size of the ChIP-seq libraries ranged from 250 to 350 bp. For multiplexing, equimolar quantities of each library were combined considering sequencing depth per sample (20 million to 40 million reads per library). The ChIP-seq libraries were then sequenced using an Illumina NextSeq platform with single-end reads of 76 bases (LAS, Seoul, Korea). For visualization with the UCSC genome browser, the makeBigWig tool (in the HOMER suite) was used to generate bigWig files.

Quantification of inflammatory cytokines

Raw234.7 cells were seeded in 12-well plates and pretreated with LPS for 8 hours. After transfection with siRNA for 30 hours, conditioned media (CM) was collected for the analysis of secreted cytokines. Cytokine concentrations were determined using a LEGENDPlex mouse inflammation panel kit (BioLegend, 740446). LEGENDPlex panels quantify the levels of candidate proteins through a bead-based immunoassay. In the assay, the CM was combined with capture beads so the specific antibodies on the beads could interact with the target proteins. The addition of detection antibodies and streptavidin-phycoerythrin produced fluorescent signal intensities in proportion to the amount of bound analyte. The experiments were conducted following the manufacturer's protocols. Data were acquired using the Attune NxT cell analyzer (Thermo Fisher Scientific) and analyzed using the LEGENDPlex software (BioLegend).

Animal experiments

Experimental colitis

To induce colitis, 8-week-old $LysM^{cre/+}$; $TAZ^{flox/flox}$ and $TAZ^{flox/flox}$ mice ($n = 7$ per group) were alternately administered 2.5% DSS (MP Biomedicals, 9011-18-1) in drinking water and regular water for 36 days. In this model, mouse body weight was monitored every 2 days until the mice were euthanized at 36 days.

Sepsis animal model

Eight-week-old $LysM^{cre/+}$; $TAZ^{flox/flox}$ and $TAZ^{flox/flox}$ male mice ($n =$ 12 per group) were intraperitoneally injected with LPS (27 mg/kg of body weight) (Sigma-Aldrich, LPS *E. coli* O111:B4). Survival rates were monitored in mice with LPS-induced sepsis for 60 hours.

Allograft

For the tumor growth assay, 8-week-old NOD/SCID and C57BL/6 J male mice were randomly assigned to two randomized groups ($n = 6$ per group). Then, B16F10 cells/siCon or B16F10 cells/siTaz (3×10^5) were injected subcutaneously into the right flank of each mouse. The mice were euthanized 3 weeks after the experiment began and their tumor tissues were further examined by hematoxylin and eosin (H&E) or imunohistochemical (IHC) staining.

Metabolic dysfunction–associated steatohepatitis

Six-week-old *LysM*$^{cre/+}$; *TAZ*$^{flox/flox}$ and *TAZ*$^{flox/flox}$ male mice were fed a choline-deficient, L-amino acid–defined, high-fat diet (CDAHFD) (Research Diets Inc., A06071302) known to induce MASH in mice with rapid development of liver fibrosis. At the 16-week mark, an insulin tolerance test (0.75 U/kg) was conducted on the mice after a 4-hour fast. At the 18-week mark, a glucose tolerance test (2 g/kg) was performed on mice that had been fasted overnight. Blood glucose levels were measured from the lateral tail vein using a glucose meter (Glucodoctor). The mice were euthanized 34 weeks after the experiment began. The liver tissues of the mice were further examined by H&E, IHC staining, or qRT-PCR.

Immunohistochemistry

Slides containing 4-μm thick sections from B16F10 tumors and mouse liver samples were dried at 62°C for 30 min and then subjected to deparaffinization. Antigen retrieval was conducted in tris-EDTA buffer at 100°C for 15 min. and then the slides were cooled at room temperature for 30 min. Peroxidase blocking was performed with 3% H_2O_2 for 15 min. Following washing, blocking of nonspecific binding was carried out with 4% BSA for 30 min. The slides were then incubated at room temperature for 1 hour with primary antibody. After washing, secondary antibody (goat anti-rabbit IgG_HRP, Abcam USA) was applied for 30 min. The stained slides were visualized using a digital slide scanner (PANNORAMIC SCAN II, 3D HISTECH, Hungary). Pathologists at T&P Bio and Professor JaeHak Park at Seoul National University College of Veterinary Medicine used the Image-Pro analysis program (Media Cybernetics Inc. USA) to independently scan and quantify all sections of each tissue. The pathologists and T&P Bio conducted separate analyses.

Statistical analysis

All quantitative data were obtained from a minimum of three independent biological replicates. Data are presented as means ± SD unless otherwise specified. Statistical differences between two groups were assessed using two-tailed, unpaired Student's *t* tests or one-way analysis of variance (ANOVA) with Bonferroni corrections for multiple comparisons. Pearson's correlation coefficient was used to analyze colocalization between fluorescence channels in confocal microscopy images. Statistical tests were conducted using the GraphPad Prism 9.0 software (GraphPad Software, CA, USA). Two-sided *P* values of less than 0.05 were considered significant. Sample sizes were not predetermined using specific statistical methods but were based on prior experience with experimental variability. Blinding procedures were implemented whenever possible during sample analysis. This included a coding of sample identities during data collection and blinding the researcher performing the data analysis to the experimental conditions.

Supplementary Materials

This PDF file includes:

Figs. S1 to S5

REFERENCES AND NOTES

1. B. Zhao, K. Tumaneng, K.-L. Guan, The Hippo pathway in organ size control, tissue regeneration and stem cell self-renewal. *Nat. Cell Biol.* **13**, 877–883 (2011).
2. K. F. Harvey, X. Zhang, D. M. Thomas, The Hippo pathway and human cancer. *Nat. Rev. Cancer* **13**, 246–257 (2013).
3. S. Moon, S. Yeon Park, H. Woo Park, Regulation of the Hippo pathway in cancer biology. *Cell. Mol. Life Sci.* **75**, 2303–2319 (2018).
4. A. Totaro, T. Panciera, S. Piccolo, YAP/TAZ upstream signals and downstream responses. *Nat. Cell Biol.* **20**, 888–899 (2018).
5. J. S. Mo, H. W. Park, K. L. Guan, The Hippo signaling pathway in stem cell biology and cancer. *EMBO Rep.* **15**, 642–656 (2014).
6. J. E. Thaventhiran, A. Hoffmann, L. Magiera, M. de la Roche, H. Lingel, M. Brunner-Weinzierl, D. T. Fearon, Activation of the Hippo pathway by CTLA-4 regulates the expression of Blimp-1 in the CD8+ T cell. *Proc. Natl. Acad. Sci. U.S.A.* **109**, E2223–E2229 (2012).
7. J. Geng, S. Yu, H. Zhao, X. Sun, X. Li, P. Wang, X. Xiong, L. Hong, C. Xie, J. Gao, Y. Shi, J. Peng, R. L. Johnson, N. Xiao, L. Lu, J. Han, D. Zhou, L. Chen, The transcriptional coactivator TAZ regulates reciprocal differentiation of T_H17 cells and T_{reg} cells. *Nat. Immunol.* **18**, 800–812 (2017).
8. S. Wang, F. Xie, F. Chu, Z. Zhang, B. Yang, T. Dai, L. Gao, L. Wang, L. Ling, J. Jia, H. van Dam, J. Jin, L. Zhang, F. Zhou, YAP antagonizes innate antiviral immunity and is targeted for lysosomal degradation through IKKε-mediated phosphorylation. *Nat. Immunol.* **18**, 733–743 (2017).
9. Y. Feng, Y. Liang, X. Zhu, M. Wang, Y. Gui, Q. Lu, M. Gu, X. Xue, X. Sun, W. He, J. Yang, R. L. Johnson, C. Dai, The signaling protein Wnt5a promotes TGFβ1-mediated macrophage polarization and kidney fibrosis by inducing the transcriptional regulators Yap/Taz. *J. Biol. Chem.* **293**, 19290–19302 (2018).
10. X. Zhou, W. Li, S. Wang, P. Zhang, Q. Wang, J. Xiao, C. Zhang, X. Zheng, X. Xu, S. Xue, L. Hui, H. Ji, B. Wei, H. Wang, YAP aggravates inflammatory bowel disease by regulating M1/M2 macrophage polarization and gut microbial homeostasis. *Cell Rep.* **27**, 1176–1189. e5 (2019).
11. V. S. Meli, H. Atcha, P. K. Veerasubramanian, R. R. Nagalla, T. U. Luu, E. Y. Chen, C. F. Guerrero-Juarez, K. Yamaga, W. Pandori, J. Y. Hsieh, T. L. Downing, D. A. Fruman, M. B. Lodoen, M. V. Plikus, W. Wang, W. F. Liu, YAP-mediated mechanotransduction tunes the macrophage inflammatory response. *Sci. Adv.* **6**, eabb8471 (2020).
12. M. M. Mia, D. M. Cibi, S. A. B. Abdul Ghani, W. Song, N. Tee, S. Ghosh, J. Mao, E. N. Olson, M. K. Singh, YAP/TAZ deficiency reprograms macrophage phenotype and improves infarct healing and cardiac function after myocardial infarction. *PLOS Biol.* **18**, e3000941 (2020).
13. K. Song, H. Kwon, C. Han, W. Chen, J. Zhang, W. Ma, S. Dash, C. R. Gandhi, T. Wu, Yes-associated protein in Kupffer cells enhances the production of proinflammatory cytokines and promotes the development of nonalcoholic steatohepatitis. *Hepatology* **72**, 72–87 (2020).
14. D. Wang, Y. Zhang, X. Xu, J. Wu, Y. Peng, J. Li, R. Luo, L. Huang, L. Liu, S. Yu, N. Zhang, B. Lu, K. Zhao, YAP promotes the activation of NLRP3 inflammasome via blocking K27-linked polyubiquitination of NLRP3. *Nat. Commun.* **12**, 2674 (2021).
15. L. Chen, X. Jin, J. Ma, B. Xiang, X. Li, YAP at the progression of inflammation. *Front. Cell Dev. Biol.* **11**, 1204033 (2023).
16. V. S. Meli, P. K. Veerasubramanian, T. L. Downing, W. Wang, W. F. Liu, Mechanosensation to inflammation: Roles for YAP/TAZ in innate immune cells. *Sci. Signal.* **16**, eadc9656 (2023).
17. M. G. Netea, F. Balkwill, M. Chonchol, F. Cominelli, M. Y. Donath, E. J. Giamarellos-Bourboulis, D. Golenbock, M. S. Gresnigt, M. T. Heneka, H. M. Hoffman, R. Hotchkiss, L. A. B. Joosten, D. L. Kastner, M. Korte, E. Latz, P. Libby, T. Mandrup-Poulsen, A. Mantovani, K. H. G. Mills, K. L. Nowak, L. A. O'Neill, P. Pickkers, T. van der Poll, P. M. Ridker, J. Schalkwijk, D. A. Schwartz, B. Siegmund, C. J. Steer, H. Tilg, J. W. M. van der Meer, F. L. van de Veerdonk, C. A. Dinarello, A guiding map for inflammation. *Nat. Immunol.* **18**, 826–831 (2017).
18. S. Chen, A. F. Saeed, Q. Liu, Q. Jiang, H. Xu, G. G. Xiao, L. Rao, Y. Duo, Macrophages in immunoregulation and therapeutics. *Signal Transduct. Target. Ther.* **8**, 207 (2023).
19. H. Zhao, L. Wu, G. Yan, Y. Chen, M. Zhou, Y. Wu, Y. Li, Inflammation and tumor progression: Signaling pathways and targeted intervention. *Signal Transduct. Target. Ther.* **6**, 263 (2021).
20. H. Li, Y. Meng, S. He, X. Tan, Y. Zhang, X. Zhang, L. Wang, W. Zheng, Macrophages, chronic inflammation, and insulin resistance. *Cells* **11**, 3001 (2022).
21. J. N. Fullerton, D. W. Gilroy, Resolution of inflammation: A new therapeutic frontier. *Nat. Rev. Drug Discov.* **15**, 551–567 (2016).
22. G. Schett, M. F. Neurath, Resolution of chronic inflammatory disease: Universal and tissue-specific concepts. *Nat. Commun.* **9**, 3261 (2018).
23. A. Mantovani, P. Allavena, A. Sica, F. Balkwill, Cancer-related inflammation. *Nature* **454**, 436–444 (2008).
24. M. Y. Donath, Targeting inflammation in the treatment of type 2 diabetes: Time to start. *Nat. Rev. Drug Discov.* **13**, 465–476 (2014).
25. W. Liang, J. H. Lindeman, A. L. Menke, D. P. Koonen, M. Morrison, L. M. Havekes, A. M. Van Den Hoek, R. Kleemann, Metabolically induced liver inflammation leads to NASH and differs from LPS-or IL-1β-induced chronic inflammation. *Lab. Invest.* **94**, 491–502 (2014).
26. J. Liu, X. Geng, J. Hou, G. Wu, New insights into M1/M2 macrophages: Key modulators in cancer progression. *Cancer Cell Int.* **21**, 389 (2021).

27. T. J. Hagenbeek, J. D. Webster, N. M. Kljavin, M. T. Chang, T. Pham, H.-J. Lee, C. Klijn, A. G. Cai, K. Totpal, B. Ravishankar, N. Yang, D.-H. Lee, K. B. Walsh, G. Hatzivassiliou, C. C. de la Cruz, S. E. Gould, X. Wu, W. P. Lee, S. Yang, Z. Zhang, Q. Gu, Q. Ji, E. L. Jackson, D.-S. Lim, A. Dey, The Hippo pathway effector TAZ induces TEAD-dependent liver inflammation and tumors. *Sci. Signal.* **11**, eaaj1757 (2018).
28. T. J. Hagenbeek, J. R. Zbieg, M. Hafner, R. Mroue, J. A. Lacap, N. M. Sodir, C. L. Noland, S. Afghani, A. Kishore, K. P. Bhat, X. Yao, S. Schmidt, S. Clausen, M. Steffek, W. Lee, P. Beroza, S. Martin, E. Lin, R. Fong, P. D. Lello, M. H. Kubala, M. N.-Y. Yang, J. T. Lau, E. Chan, A. Arrazate, L. An, E. Levy, M. N. Lorenzo, H.-J. Lee, T. H. Pham, Z. Modrusan, R. Zang, Y.-C. Chen, M. Kabza, M. Ahmed, J. Li, M. T. Chang, D. Maddalo, M. Evangelista, X. Ye, J. J. Crawford, A. Dey, An allosteric pan-TEAD inhibitor blocks oncogenic YAP/TAZ signaling and overcomes KRAS G12C inhibitor resistance. *Nat. Cancer* **4**, 812–828 (2023).
29. A. V. Pobbati, R. Kumar, B. P. Rubin, W. Hong, Therapeutic targeting of TEAD transcription factors in cancer. *Trends Biochem. Sci.* **48**, 450–462 (2023).
30. J. E. Shin, S.-H. Kim, M. Kong, H.-R. Kim, S. Yoon, K.-M. Kee, J. A. Kim, D. H. Kim, S. Y. Park, J. H. Park, H. Kim, K. T. No, H.-W. Lee, H. Y. Gee, S. Hong, K.-L. Guan, J.-S. Roe, H. Lee, D.-W. Kim, H. W. Park, Targeting FLT3-TAZ signaling to suppress drug resistance in blast phase chronic myeloid leukemia. *Mol. Cancer* **22**, 177 (2023).
31. T. Kawai, S. Akira, The role of pattern-recognition receptors in innate immunity: Update on Toll-like receptors. *Nat. Immunol.* **11**, 373–384 (2010).
32. K. A. Fitzgerald, J. C. Kagan, Toll-like receptors and the control of immunity. *Cell* **180**, 1044–1066 (2020).
33. M. Shreberk-Shaked, M. Oren, New insights into YAP/TAZ nucleo-cytoplasmic shuttling: New cancer therapeutic opportunities? *Mol. Oncol.* **13**, 1335–1341 (2019).
34. J. Rehwinkel, M. U. Gack, RIG-I-like receptors: Their regulation and roles in RNA sensing. *Nat. Rev. Immunol.* **20**, 537–551 (2020).
35. K. C. Lin, T. Moroishi, Z. Meng, H.-S. Jeong, S. W. Plouffe, Y. Sekido, J. Han, H. W. Park, K.-L. Guan, Regulation of Hippo pathway transcription factor TEAD by p38 MAPK-induced cytoplasmic translocation. *Nat. Cell Biol.* **19**, 996–1002 (2017).
36. S. W. Plouffe, K. C. Lin, J. L. Moore, F. E. Tan, S. Ma, Z. Ye, Y. Qiu, B. Ren, K.-L. Guan, The Hippo pathway effector proteins YAP and TAZ have both distinct and overlapping functions in the cell. *J. Biol. Chem.* **293**, 11230–11240 (2018).
37. T. T. Tang, A. W. Konradi, Y. Feng, X. Peng, M. Ma, J. Li, F.-X. Yu, K.-L. Guan, L. Post, Small molecule inhibitors of TEAD auto-palmitoylation selectively inhibit proliferation and tumor growth of NF2-deficient mesothelioma. *Mol. Cancer Ther.* **20**, 986–998 (2021).
38. N. Young, G. Punkosdy, J. Cavanaugh, C. Bantle, A. Constan, B. Li, J. Conley, M. Sanchez-Martin, L. Xu, K. McGovern, A. Castro, M. Zhang, J. Ecsedy, IK-930, a paralog-selective TEAD inhibitor for treating YAP/TAZ-TEAD dependent cancers. *Cancer Res.* **83**, 1646 (2023).
39. J. Xu, P. J. Vanderzalm, M. Ludwig, T. Su, S. A. Tokamov, R. G. Fehon, Yorkie functions at the cell cortex to promote myosin activation in a non-transcriptional manner. *Dev. Cell* **46**, 271–284. e5 (2018).
40. J. Yuan, X. Dong, J. Yap, J. Hu, The MAPK and AMPK signalings: Interplay and implication in targeted cancer therapy. *J. Hematol. Oncol.* **13**, 113 (2020).
41. M. Xin, Y. Kim, L. B. Sutherland, M. Murakami, X. Qi, J. McAnally, E. R. Porrello, A. I. Mahmoud, W. Tan, J. M. Shelton, J. A. Richardson, H. A. Sadek, R. Bassel-Duby, E. N. Olson, Hippo pathway effector Yap promotes cardiac regeneration. *Proc. Natl. Acad. Sci. U.S.A.* **110**, 13839–13844 (2013).
42. Y.-L. Hung, S.-H. Fang, S.-C. Wang, W.-C. Cheng, P.-L. Liu, C.-C. Su, C.-S. Chen, M.-Y. Huang, K.-F. Hua, K.-H. Shen, Y.-T. Wang, K. Suzuki, C.-Y. Li, Corylin protects LPS-induced sepsis and attenuates LPS-induced inflammatory response. *Sci. Rep.* **7**, 46299 (2017).
43. S. Talley, R. Valiauga, L. Anderson, A. R. Cannon, M. A. Choudhry, E. M. Campbell, DSS-induced inflammation in the colon drives a proinflammatory signature in the brain that is ameliorated by prophylactic treatment with the S100A9 inhibitor paquinimod. *J. Neuroinflammation* **18**, 263 (2021).
44. T. Xia, M. Zhang, W. Lei, R. Yang, S. Fu, Z. Fan, Y. Yang, T. Zhang, Advances in the role of STAT3 in macrophage polarization. *Front. Immunol.* **14**, 1160719 (2023).
45. J. S. Dolina, N. Van Braeckel-Budimir, G. D. Thomas, S. Salek-Ardakani, $CD8^+$ T cell exhaustion in cancer. *Front. Immunol.* **12**, 715234 (2021).
46. X. Wang, Z. Zheng, J. M. Caviglia, K. E. Corey, T. M. Herfel, B. Cai, R. Masia, R. T. Chung, J. H. Lefkowitch, R. F. Schwabe, I. Tabas, Hepatocyte TAZ/WWTR1 promotes inflammation and fibrosis in nonalcoholic steatohepatitis. *Cell Metab.* **24**, 848–862 (2016).
47. M. Mooring, B. H. Fowl, S. Z. Lum, Y. Liu, K. Yao, S. Softic, R. Kirchner, A. Bernstein, A. D. Singhi, D. G. Jay, C. R. Kahn, F. D. Camargo, D. Yimlamai, Hepatocyte stress increases expression of yes-associated protein and transcriptional coactivator with PDZ-binding motif in hepatocytes to promote parenchymal inflammation and fibrosis. *Hepatology* **71**, 1813–1830 (2020).
48. X. Wang, B. Cai, X. Yang, O. O. Sonubi, Z. Zheng, R. Ramakrishnan, H. Shi, L. Valenti, U. B. Pajvani, J. Sandhu, R. E. Infante, A. Radhakrishnan, D. F. Covey, K.-L. Guan, J. Buck, L. R. Levin, P. Tontonoz, R. F. Schwabe, I. Tabas, Cholesterol stabilizes TAZ in hepatocytes to promote experimental non-alcoholic steatohepatitis. *Cell Metab.* **31**, 969–986. e7 (2020).
49. A. Yu, C. Cable, S. Sharma, M. H. Shihan, A. N. Mattis, I. Mileva, Y. A. Hannun, C. C. Duwaerts, J. Y. Chen, Targeting acid ceramidase ameliorates fibrosis in mouse models of non-alcoholic steatohepatitis. *Front. Med.* **9**, 881848 (2022).
50. H. D. Huh, Y. Sub, J. Oh, Y. E. Kim, J. Y. Lee, H.-R. Kim, S. Lee, H. Lee, S. Pak, S. E. Amos, D. Vahala, J. H. Park, J. E. Shin, S. Y. Park, H. S. Kim, Y. H. Roh, H.-W. Lee, K.-L. Guan, Y. S. Choi, J. Jeong, J. Choi, J.-S. Roe, H. Y. Gee, H. W. Park, Reprogramming anchorage dependency by adherent-to-suspension transition promotes metastatic dissemination. *Mol. Cancer* **22**, 63 (2023).
51. Y. Wang, A. H. van Boxel-Dezaire, H. Cheon, J. Yang, G. R. Stark, STAT3 activation in response to IL-6 is prolonged by the binding of IL-6 receptor to EGF receptor. *Proc. Natl. Acad. Sci. U.S.A.* **110**, 16975–16980 (2013).
52. S. Zou, Q. Tong, B. Liu, W. Huang, Y. Tian, X. Fu, Targeting STAT3 in cancer immunotherapy. *Mol. Cancer* **19**, 145 (2020).
53. M. S. Paul, P. S. Ohashi, The roles of $CD8^+$ T cell subsets in antitumor immunity. *Trends Cell Biol.* **30**, 695–704 (2020).
54. N. L. Stevenson, D. J. Bergen, R. E. Skinner, E. Kague, E. Martin-Silverstone, K. A. Robson Brown, C. L. Hammond, D. J. Stephens, Giantin-knockout models reveal a feedback loop between Golgi function and glycosyltransferase expression. *J. Cell Sci.* **130**, 4132–4143 (2017).
55. R.-M. Hsu, C.-Y. Zhong, C.-L. Wang, W.-C. Liao, C. Yang, S.-Y. Lin, J.-W. Lin, H.-Y. Cheng, P.-Y. Li, C.-J. Yu, Golgi tethering factor golgin-97 suppresses breast cancer cell invasiveness by modulating NF-κB activity. *Cell Commun. Signal* **16**, 19 (2018).
56. Y. Liu, X. Zhang, S. Zhou, J. Shi, Y. Xu, J. He, F. Lin, A. Wei, L. Zhou, Z. Chen, Knockdown of Golgi phosphoprotein 73 blocks the trafficking of matrix metalloproteinase-2 in hepatocellular carcinoma cells and inhibits cell invasion. *J. Cellular Mol. Med.* **23**, 2399–2409 (2019).

Acknowledgments

Funding: This work was supported by grants from the National Research Foundation of Korea (2020M3F7A1094077, 2020M3F7A1094089, 2021R1A2C1010828, and RS-2024-00509461 to H.W.P. and RS-2023-00208127 and RS-2023-00260454 to S.-Y.P.), by Global–Learning & Academic research institution for Master's PhD students and Postdocs (LAMP) Program of the National Research Foundation of Korea grant funded by the Ministry of Education (RS-2024-00442483 to H.W.P.), and by the Brain Korea 21 FOUR Program (to S.Y.P., D.H.K., H.-R.K., S.C.C., and J.E.P.). **Author contributions:** Conceptualization: S.Y.P., H.W.P., S.-Y.P., K.-L.G., D.H.K., J.E.S., and S.C.C. Methodology: S.Y.P., H.W.P., S.-Y.P., K.-L.G., S.-J.H., D.J.P., H.G.K., K.-H.C., H.-W.L., and J.L. Software: S.Y.P. and H.W.P. Validation: S.Y.P., H.W.P., S.-J.H., S.-Y.P., D.J.P., J.C., H.S., and D.H.K. Formal analysis: S.Y.P., H.W.P., Y.S., S.-Y.P., J.-S.R., H.-R.K., H.Y.G., D.H.K., Y.-J.K., D.K., and H.S. Investigation: S.Y.P., H.W.P., S.-Y.P., Y.S., D.J.P., J.-S.R., H.-R.K., H.S., J.E.P., H.Y.G., S.P., H.G.K., K.-H.C., S.C.C., H.-W.L., J.L., and S.J. Resources: S.Y.P., H.W.P., S.-J.H., S.-Y.P., D.J.P., H.S., D.H.K., J.C., Y.-J.K., K.-H.C., H.-W.L., and J.L. Data curation: S.Y.P., H.W.P., Y.S., and D.H.K. Writing—original draft: S.Y.P. and H.W.P. Writing—review and editing: S.Y.P., H.W.P., J.E.S., and S.C.C. Visualization: S.Y.P., H.W.P., and Y.S. Supervision: S.Y.P., H.W.P., and K.-L.G. Project administration: S.Y.P. and H.W.P. Funding acquisition: S.Y.P., H.W.P., and S.-Y.P. **Competing interests:** K.-L.G. is a cofounder of Vivace Therapeutics and a scientific advisor of OncoC4 Inc. and Shanghai Henlius Biotech Inc. The authors declare no other competing interests. **Data and materials availability:** The RNA-seq data reported in this study are available in the Gene Expression Omnibus (GEO) database under KAP240685. All data needed to evaluate the conclusions in the paper are present in the paper and/or the Supplementary Materials.

Submitted 5 May 2024
Accepted 19 December 2024
Published 22 January 2025
10.1126/sciadv.adq2395